Atmos. Chem. Phys., 18, 1475–1494, 2018
https://doi.org/10.5194/acp-18-1475-2018

Atmospheric Chemistry and Physics
Open Access
EGU

Relating large-scale subsidence to convection development in Arctic mixed-phase marine stratocumulus

Gillian Young[1,a], **Paul J. Connolly**[1], **Christopher Dearden**[1,b], **and Thomas W. Choularton**[1]

[1]Centre for Atmospheric Science, School of Earth and Environmental Sciences, University of Manchester, Manchester, UK
[a]now at: British Antarctic Survey, High Cross, Madingley Road, Cambridge, UK
[b]now at: School of Earth and Environment, The University of Leeds, Leeds, UK

Correspondence: Thomas W. Choularton (choularton@manchester.ac.uk) and Gillian Young (giyoung@bas.ac.uk)

Received: 27 June 2017 – Discussion started: 18 August 2017
Revised: 22 November 2017 – Accepted: 18 December 2017 – Published: 2 February 2018

Abstract. Large-scale subsidence, associated with high-pressure systems, is often imposed in large-eddy simulation (LES) models to maintain the height of boundary layer (BL) clouds. Previous studies have considered the influence of subsidence on warm liquid clouds in subtropical regions; however, the relationship between subsidence and mixed-phase cloud microphysics has not specifically been studied. For the first time, we investigate how widespread subsidence associated with synoptic-scale meteorological features can affect the microphysics of Arctic mixed-phase marine stratocumulus (Sc) clouds. Modelled with LES, four idealised scenarios – a stable Sc, varied droplet (N_{drop}) or ice (N_{ice}) number concentrations, and a warming surface (representing motion southwards) – were subjected to different levels of subsidence to investigate the cloud microphysical response. We find strong sensitivities to large-scale subsidence, indicating that high-pressure systems in the ocean-exposed Arctic regions have the potential to generate turbulence and changes in cloud microphysics in any resident BL mixed-phase clouds.

Increased cloud convection is modelled with increased subsidence, driven by longwave radiative cooling at cloud top and rain evaporative cooling and latent heating from snow growth below cloud. Subsidence strengthens the BL temperature inversion, thus reducing entrainment and allowing the liquid- and ice-water paths (LWPs, IWPs) to increase. Through increased cloud-top radiative cooling and subsequent convective overturning, precipitation production is enhanced: rain particle number concentrations (N_{rain}), in-cloud rain mass production rates, and below-cloud evaporation rates increase with increased subsidence.

Ice number concentrations (N_{ice}) play an important role, as greater concentrations suppress the liquid phase; therefore, N_{ice} acts to mediate the strength of turbulent overturning promoted by increased subsidence. With a warming surface, a lack of – or low – subsidence allows for rapid BL turbulent kinetic energy (TKE) coupling, leading to a heterogeneous cloud layer, cloud-top ascent, and cumuli formation below the Sc cloud. In these scenarios, higher levels of subsidence act to stabilise the Sc layer, where the combination of these two forcings counteract one another to produce a stable, yet dynamic, cloud layer.

1 Introduction

Arctic mixed-phase clouds are long-lived, and widespread single-layer stratocumulus (Sc) decks are common in the autumn, winter, and spring. These clouds are maintained and driven by convection caused by strong radiative cooling at the boundary layer (BL) inversion (e.g. Feingold et al., 2010; Morrison et al., 2012). In numerical models, mechanisms affecting the break-up of these Sc clouds – including glaciation (e.g. Harrington et al., 1999; Prenni et al., 2007; Young et al., 2017) or break-up into convective cumulus (as occurs in cold-air outbreaks, CAOs) – are often too efficient, leading to radiative biases in the polar regions (Trenberth and Fasullo, 2010; Karlsson and Svensson, 2011; Bodas-Salcedo et al., 2012; de Boer et al., 2014).

Several studies (e.g. Harrington et al., 1999; Harrington and Olsson, 2001; Prenni et al., 2007; Morrison et al., 2012; de Boer et al., 2011; Young et al., 2017) have addressed the

issue of premature glaciation of modelled mixed-phase Sc, often concluding that the cause is an overactive ice phase and strong influence of the Wegener–Bergeron–Findeisen (WBF) mechanism. The WBF mechanism causes a constantly changing, unstable microphysical structure; however, these clouds have been observed to persist for long periods of time, and thus they have the opportunity to move geographically.

In a CAO, stable Arctic Sc decks are transported southwards from over the sea ice to over the warm ocean. These clouds often display closed-cellular structure at first, where narrow downdraught rings surround broad updraught columns (Schröter et al., 2005; Feingold et al., 2010). Increased sensible heat fluxes and BL depth (Young et al., 2016) promote the development of precipitation through increased cloud turbulence (Müller and Chlond, 1996). Transitions between closed- and open-cellular convection have been the focus of several studies, many of which consider warm, ice-free clouds (e.g. Wang and Feingold, 2009b; Feingold et al., 2010; Wood et al., 2011). Factors controlling this transition in CAOs are poorly understood, where the mixed-phase state of the clouds adds further complexity.

In warm clouds, cleaner scenarios (with lower aerosol particle and cloud droplet number concentrations) are susceptible to the formation of open cells due to efficient precipitation development (Feingold et al., 2010; Wang and Feingold, 2009a; Wood et al., 2011; Rosenfeld et al., 2012). However, drizzle formation has been found to be influenced more so by larger-scale meteorology, such as moisture fluxes and temperature fluctuations, than aerosol–cloud interactions (Wang et al., 2010). Similarly in CAOs, thermodynamic interactions – namely diabatic processes such as latent heat release from condensation and cloud-top radiative cooling – have been shown to strongly influence the broadening of convective cells (Müller and Chlond, 1996; Schröter et al., 2005). Such interactions are also thought to have an important role in generating dynamical overturning in the persistent mixed-phase Sc upstream in CAOs.

Regions of high surface pressure are often found upstream of CAOs in the European Arctic (Walsh et al., 2001; Fletcher et al., 2016). In the high Arctic ($\geq 80^\circ$ N, over sea ice), such regions contribute towards reduced cloud fractions (Kay and Gettelman, 2009; Stramler et al., 2011; Morrison et al., 2012). High-pressure systems are associated with large-scale subsidence and, in turn, strong BL inversions (Myers and Norris, 2013). In warm marine environments, such inversions have been shown to lead to a shallow BL depth, increased cloudiness, and increased BL mixing (Myers and Norris, 2013). Previous studies suggest that large-scale subsidence may affect CAO cellular transitions (e.g. Müller and Chlond, 1996; Feingold et al., 2015) and can even reduce the lifetime of liquid marine Sc modelled over a warming surface (van der Dussen et al., 2016). Subsidence associated with synoptic-scale meteorological features therefore has the potential to influence the microphysical evolution of BL clouds; however, the relationship between subsidence and mixed-phase cloud microphysics has not yet been studied.

The role of microphysics–dynamics interactions in sustaining microphysically unstable Arctic mixed-phase Sc is poorly understood; therefore, it is imperative to assess such feedbacks to gain a holistic view of their role in the Arctic system. By studying the cloud microphysical response to external stressors, such as large-scale subsidence, we can better evaluate the influence of environmental factors on the lifetime of mixed-phase Sc in the Arctic. Here, we investigate the influence of subsidence on a stable cloud, precipitating clouds, and a cloud forced by a warming surface to demonstrate how subsidence can affect a variation of microphysical scenarios common to the Arctic. By doing so, we will show which microphysical feedbacks are affected by subsidence and test how the combination of subsidence and a warming surface can affect BL development.

2 Methods

2.1 Model set-up

We use the UK Met Office Large Eddy Model (LEM, Gray et al., 2001) to investigate the influence of large-scale subsidence on mixed-phase marine Sc cloud microphysics. The set up is the same as that used by Young et al. (2017), whose study gives further details on the model itself. Momentum is conserved using the Piacsek–Williams (PW; Piacsek and Williams, 1970) centred difference scheme, whilst the total variation diminishing (TVD) monotonicity-preserving scheme of Leonard et al. (1993), known as ULTIMATE, is used for scalar advection (Gray et al., 2001; Shipway and Hill, 2012).

Cyclical boundary conditions and a damping layer (500 m below model lid) were imposed. Vertical profiles of potential temperature (Θ), water vapour mixing ratio (Q_{vap}), and wind speed (U and V) were implemented to initialise the model (Fig. 1): these profiles were extracted from previous LEM runs of Arctic mixed-phase Sc, specifically from 10 h in the ocean case detailed by Young et al. (2017), where a primary ice parameterisation derived from observations from the Aerosol-Cloud Coupling and Climate Interactions in the Arctic (ACCACIA) campaign was implemented. These fields give a stable BL experiencing strong (approximately 10–15 m s^{-1}) N–S winds. A humidity inversion, coinciding with the BL temperature inversion, is present in the initial Q_{vap} field (Fig. 1a): previous studies (e.g. Curry et al., 1988; Solomon et al., 2011) have shown that such inversions are often observed in the Arctic and may act as a source of moisture to BL clouds below. Surface sensible and latent heat fluxes were calculated by the model, using near-surface Θ and Q_{vap} values, to represent an oceanic surface. The Morrison et al. (2005) microphysics scheme was used, providing

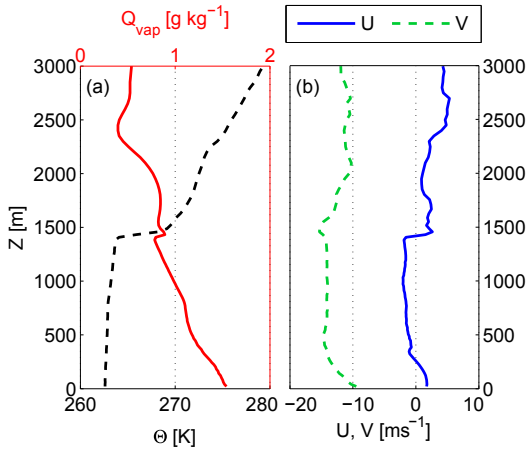

Figure 1. Profiles of potential temperature (Θ), water vapour mixing ratio (Q_{vap}), and wind speed (U, V) used to initialise the LEM.

single-moment liquid (with a prescribed droplet number) and double-moment ice, snow, graupel, and rain.

In large-eddy simulation (LES) models, large-scale subsidence (W_{sub}) is often imposed as a tuning factor to maintain cloud-top height. In such models, W_{sub} is usually calculated from an imposed large-scale horizontal divergence. In practice, a constant divergence is assumed below the BL temperature inversion – with zero divergence above – producing a linear increase in W_{sub} with height below the inversion and a constant vertical wind above it (Ovchinnikov et al., 2014; Solomon et al., 2015). Here, we calculate W_{sub} using this method, increasing linearly with altitude up to 1500 m. At altitudes > 1500 m, $W_{sub} = W_{sub}$ (1500 m) (representing zero divergence aloft).

In the literature, the imposed horizontal divergence in LES studies often ranges from 2.5×10^{-6} (Solomon et al., 2015), through 3.75×10^{-6} (Wang and Feingold, 2009a; Feingold et al., 2015; Yamaguchi and Feingold, 2015), to $5 \times 10^{-6}\,s^{-1}$ (Ovchinnikov et al., 2011). In this study, three different levels of imposed divergence – 0, 2.5×10^{-6}, and $5 \times 10^{-6}\,s^{-1}$ – are used in four separate tests to investigate the role of large-scale subsidence in both stable and precipitation-favouring microphysical scenarios. The first three scenarios give an indication of how subsidence can affect the microphysics of Arctic mixed-phase clouds that remain at approximately the same latitude, whilst the fourth considers geographical movement. Details of the tests conducted are listed in Table 1. The control simulations apply no large-scale subsidence, apply a prescribed droplet number concentration (N_{drop}) of 100 cm^{-3}, and use the DeMott et al. (2010) (hereafter, D10) parameterisation for primary ice nucleation. As in Young et al. (2017), an approximation of the D10 parameterisation is used, where we assume an aerosol particle number concentration of 2.20 cm^{-3} (for implementation in the parameterisation) throughout the domain.

Test 1 (Sect. 3.1) considers the effect of imposing different levels of subsidence on the microphysical properties of a stable mixed-phase Sc layer. In Sect. 3.2 and 3.3, parameters relating to development of precipitation in the liquid or ice phase are varied to test the microphysical response under different levels of large-scale subsidence. For example, we expect to enhance rain formation by decreasing N_{drop} (test 2, Sect. 3.2) and increase snow formation by increasing N_{ice} (test 3, Sect. 3.3). However, decreasing N_{ice} should sustain the liquid phase against the WBF mechanism, also likely affecting rain formation. Therefore, test 3 has the potential to affect both phases in the modelled clouds.

Test 4 investigates larger-scale BL interactions with a stable mixed-phase Sc layer. In CAOs, clouds move southwards off the sea ice and thus are subjected to a warming ocean surface. Model simulations in tests 1, 2, and 3 do not include any surface forcing: surface temperatures are allowed to vary through feedbacks with the BL above, yet they are not monotonically forced to become warmer. Such a forcing is applied in test 4 to investigate the combined influence of subsidence and a warming surface, simulating motion southwards. Near-surface temperatures are kept constant at 263.48 K until 5 h to allow adequate time for model spin-up, after which they are forced to warm linearly, in hourly increments, to 265.66 K at approximately 11 h 20 min. This warming profile was artificially constructed based on approximated ERA-Interim (ECMWF reanalysis; Dee et al., 2011) 2 m temperature variations over the ocean in the Svalbard archipelago, close to the sea ice, during a cold-air outbreak (23 March 2013; see Young et al., 2016, 2017, and Fig. S1 in the Supplement for further details).

We employ a horizontal resolution of 120 m over a 16 km × 16 km domain centred on 71° N in the European Arctic to allow appropriate shortwave (SW) radiation calculations to be made by the model. Vertical resolution for the majority of model simulations was 20 m up to 1500 m, decreasing to 50 m between 1500 and 3000 m (domain lid) to reduce computational cost. A second domain structure was tested to check sensitivities to this set up: the high-resolution region was extended to 2300 m (again, reducing to 50 m above this height). Whilst our results are largely unaffected by the introduction of more vertical levels (not shown; see Fig. S2), this modified domain structure was applied in Sect. 3.4 (test 4) due to increasing cloud height.

3 Results

3.1 Test 1: stable stratocumulus

Firstly, the influence of large-scale subsidence on the evolution of a stable mixed-phase marine Sc is examined. Prescribed droplet number concentrations and parameterised primary ice nucleation were not altered.

Table 1. Simulation list.

Test number	Run label	Horizontal divergence [s^{-1}]	Prescribed N_{drop} [cm^{-3}]	N_{ice} parameterisation	Surface forcing [Y/N]*
1	CNTRL	OFF	100	D10	N
1	LOSUB	2.5×10^{-6}	100	D10	N
1	HISUB	5.0×10^{-6}	100	D10	N
2	CNTRL_Ndrop50/150	OFF	50/150	D10	N
2	LOSUB_Ndrop50/150	2.5×10^{-6}	50/150	D10	N
2	HISUB_Ndrop50/150	5.0×10^{-6}	50/150	D10	N
3	CNTRL_D10x0.5/2	OFF	100	D10 × 0.5/2	N
3	LOSUB_D10x0.5/2	2.5×10^{-6}	100	D10 × 0.5/2	N
3	HISUB_D10x0.5/2	5.0×10^{-6}	100	D10 × 0.5/2	N
4	CNTRL_SURFWARM	OFF	100	D10	Y
4	LOSUB_SURFWARM	2.5×10^{-6}	100	D10	Y
4	HISUB_SURFWARM	5.0×10^{-6}	100	D10	Y

* See text for further details.

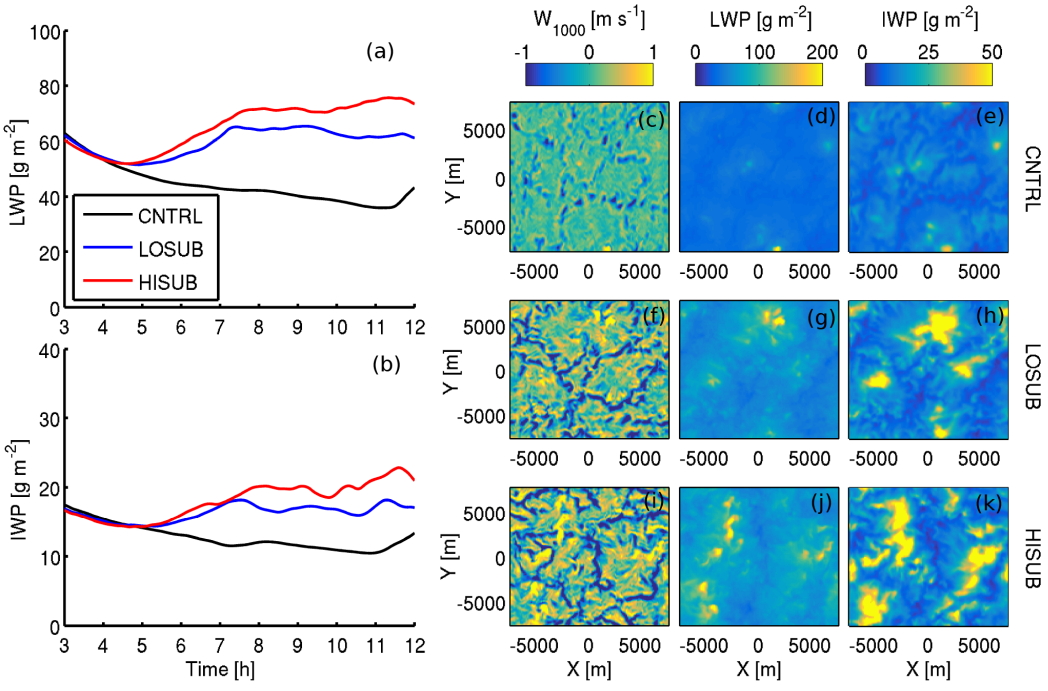

Figure 2. (a, b) Time series of the domain-averaged LWP and IWP from simulations imposing different magnitudes of large-scale subsidence. Black: control cases; blue: low W_{sub} (LOSUB); red: high W_{sub} (HISUB). **(c–k)** Planar X–Y views of **(c, f, j)** vertical velocity at 1000 m (W_{1000}), **(d, g, j)** LWP, and **(e, h, k)** IWP. Planar views shown at 11 h.

In all cases, the modelled clouds display the typical representation of a liquid-topped Arctic single-layer mixed-phase Sc, with heterogeneous ice number concentrations spread throughout the cloud below (not shown, Figs. S3–S5). Domain-averaged liquid- and ice-water paths (LWPs, IWPs) are shown in Fig. 2a and b, where the first 3 h of each simulation is excluded due to model spin-up. A stable Sc is modelled in the absence of W_{sub} (CNTRL, Fig. 2a). Increasing W_{sub} (LOSUB: low W_{sub}; HISUB: high W_{sub}) strengthens the temperature inversion, as shown in Table 2, thus reducing entrainment into the cloud from above the BL. Consequently, both the LWP and the IWP increase after approximately 5 h. These traces become more variable with time when subsidence is imposed, as is particularly visible in

the IWP traces, suggesting increased dynamic activity in the modelled clouds. Longwave (LW) radiative cooling is instrumental in allowing this convection to develop (Fig. S6).

Planar X–Y views of the vertical velocity at 1000 m (W_{1000}), LWP, and IWP fields at 11 h (Fig. 2c–k) further illustrate the effect subsidence has on the spatial structure of the clouds. With increasing W_{sub}, numerous regions of high LWP/IWP develop, with heightened heterogeneity across the domain. Domain-wide variability in W_{1000} also increases with W_{sub}. Broad updraught regions surrounded by narrow downdraught rings become apparent. Localised regions of high LWP and IWP can be associated with strong updraughts at 1000 m, and lower IWPs mirror the shape of the downdraught rings around the updraught regions. This locality becomes clearer with increasing W_{sub} (Fig. 2i, k).

Figure 3 shows a time series of turbulent kinetic energy (TKE) in panels a–c and vertical profiles of key properties in panels d–i. Increasing W_{sub} increases the snow and graupel mass tendencies below cloud (Fig. 3d). Strong snow sublimation is simulated at cloud top in all cases, with steady snow production in and below cloud. Regions of enhanced $\delta Q_{\mathrm{sg}}/\delta t$ coincide with strong rain evaporation (Fig. 3e); all of the rain produced evaporates below cloud, and no rain mass reaches the surface. Precipitation as snow does reach the surface; however, the spatial distribution becomes more heterogeneous with increased W_{sub} (not shown, Figs. S3–S5). Observational studies of Arctic mixed-phase marine Sc (Young et al., 2016) and North Atlantic CAOs (Abel et al., 2017) have previously reported precipitation as snow below cloud with little rain measured, indicating that our idealised study is in broad agreement with measurements in this region.

A downward flux of heat and moisture into cloud top is modelled in all cases, caused by the temperature and humidity inversions (Fig. 3h, i): with increased levels of W_{sub}, $w'\Theta'$ increases more so in the sub-cloud layer, whilst $w'Q'_{\mathrm{vap}}$ increases throughout the BL. Sub-cloud enhancement of $w'\Theta'$ coincides with the top of regions of enhanced snow and graupel mass growth (Fig. 3d). Modelled ice–liquid potential temperatures (Θ_{il}, following Tripoli and Cotton, 1981; Bryan and Fritsch, 2004) in the LO- and HISUB cases are colder than the CNTRL throughout the BL (Fig. 3f). All cases display a stable BL structure in the lower 1200 m of the BL and an unstable structure within cloud. A minor inversion is modelled at approximately 500 m in the CNTRL case which is co-located with a total water mixing ratio (Q_{tot}) inversion and a moist surface layer (Fig. 3a).

TKE increases throughout the BL with increasing subsidence (Fig. 3b, c) and peaks at cloud top in all cases, likely influenced by the high evaporation and sublimations rates of rain and snow at the BL-capping temperature inversion. In all simulations, TKE typically increases with altitude through the BL. When subsidence is imposed, these TKE profiles tend towards a coupled, well-mixed BL through the top-down and bottom-up propagation of TKE. This coupling is particularly clear in the HISUB case (Fig. 3c); however, the cloud-top peak in TKE remains dominant throughout every case. Increasing W_{sub} produces a more coupled, dynamic BL due to a heightened LWP, efficient LW radiative cooling, and increased rain evaporation and snow growth below cloud.

3.2 Test 2: droplet number concentration

The influence of large-scale subsidence on the formation of rain in a mixed-phase marine Sc is now considered. Prescribed droplet number concentrations were varied to a lower ($N_{\mathrm{drop}} = 50\,\mathrm{cm}^{-3}$) and higher ($N_{\mathrm{drop}} = 150\,\mathrm{cm}^{-3}$) threshold to affect rain formation: the modelled liquid mass is distributed amongst this concentration, such that a lower (higher) concentration will yield larger (smaller) cloud drops. Therefore, we expect the lower concentration of cloud droplets to allow for more efficient rain formation. Sandu and Stevens (2011) conducted a similar sensitivity study when studying Sc-to-cumulus transitions with an LES model and found that decreasing droplet number concentrations, and enhancing precipitation, significantly affected the transition efficiency.

From Fig. 4a, the Ndrop50 scenarios produce a slightly greater LWP and IWP after 8 h than Ndrop100 or Ndrop150. Increasing N_{drop} has little effect on the LWP or IWP; the results of the Ndrop100 and Ndrop150 cases are remarkably similar. Additionally, changing N_{drop} has little effect on the depth of the cloud layer modelled in the CNTRL cases (shown by shading in Fig. 4c–k). In general, varying W_{sub} affects the modelled LWP, IWP, and dynamical fluxes more than the microphysical changes (varying N_{drop}).

Figure 5 shows the mass production and sublimation/evaporation rates of snow/graupel and rain relative to the CNTRL in panels A and B respectively. Absolute domain-averaged number concentrations from each subsidence simulation are overlaid as contours. Varying N_{drop} has only a minor effect on the time evolution of the snow and graupel number concentration (N_{sg}). Snow mass production rates (relative to the CNTRL) increase towards cloud base and below cloud with increasing W_{sub}, whilst snow sublimation rates at cloud top also increase. Non-zero snow concentrations reach the surface in all simulations (Fig. 5A).

Figure 5B shows a contrasting trend for rain production/evaporation. Decreasing N_{drop} strongly affects N_{rain} as expected; for example, N_{rain} increases by approximately $9\,\mathrm{L}^{-1}$ between the HISUB_Ndrop100 and HISUB_Ndrop50 cases. For the LOSUB comparison, N_{rain} increases by approximately $6\,\mathrm{L}^{-1}$ in cloud. Increasing W_{sub} enhances the N_{rain} produced by decreasing N_{drop} in the modelled cloud. $\delta Q_{\mathrm{sg}}/\delta t$ at cloud base, relative to the CNTRLs, does not change significantly when changing N_{drop}, even with strengthened rain mass evaporation in this region; however, the below-cloud enhancement of $\delta Q_{\mathrm{sg}}/\delta t$ by increasing W_{sub} is apparent in each case.

Table 2. Key BL and cloud microphysical parameters affected by large-scale subsidence in test 1. $\Delta\Theta_{il}$ is calculated across the BL inversion and is listed to illustrate the inversion strength. Peak mass sublimation/evaporation and production rates are quoted at 9 h, comparable with Fig. 3.

Run label	Peak TKE[a,b] [$m^2\ s^{-2}$]	$\Delta\Theta_{il}$ [K]	Peak LWP[b] [$g\ m^{-2}$]	Peak IWP[b] [$g\ m^{-2}$]	Min/Max $\delta Q_{sg}/\delta t$ [$g\ kg^{-1}\ h^{-1}$]	Min[c]/Max $\delta Q_{rain}/\delta t$ [$g\ kg^{-1}\ h^{-1}$]
CNTRL	1.0	7.52	62.9	17.5	−0.059/0.010	-2.9×10^{-4}/1.3×10^{-4}
LOSUB	1.3	7.74	65.4	18.2	−0.119/0.025	-5.2×10^{-4}/2.5×10^{-4}
HISUB	1.7	7.84	75.6	22.8	−0.158/0.041	-8.1×10^{-4}/2.9×10^{-4}

[a] At cloud top. [b] Maximum values attained within 12 h simulation time. [c] Minimum below cloud.

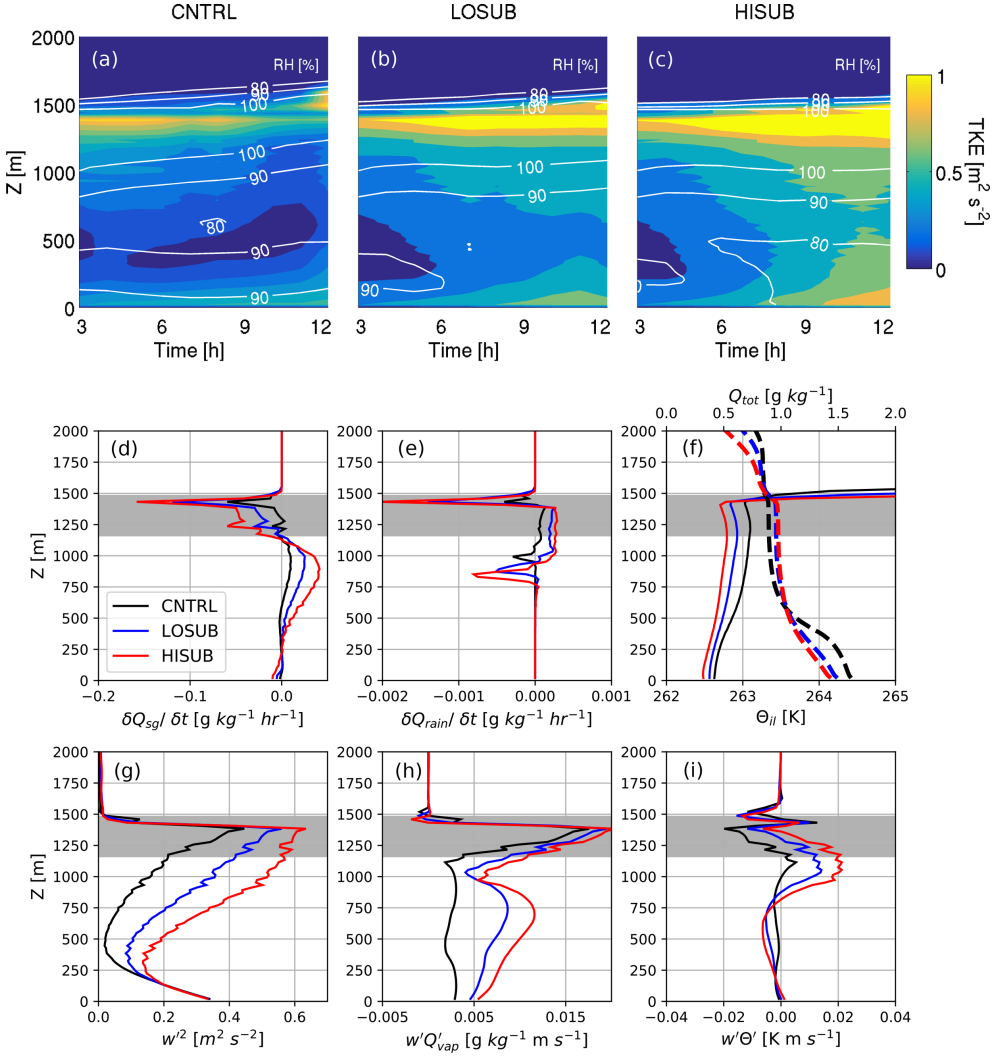

Figure 3. (a–c) Total turbulent kinetic energy (TKE, shading) and relative humidity (RH, white contours) time series for differing levels of subsidence. **(d–i)** Vertical profiles, at 9 h, of **(d)** solid precipitation (snow + graupel) mass tendency ($\delta Q_{sg}/\delta t$), **(e)** rain mass tendency ($\delta Q_{rain}/\delta t$), **(f)** ice–liquid potential temperature (Θ_{il}, solid) and total water mixing ratio (Q_{tot}, bold dashed), **(g)** vertical velocity variance (w'^2), **(h)** vertical flux of water vapour ($w'Q'_{vap}$), and **(i)** buoyancy flux ($w'\Theta'$). **(g–i)** w'^2, $w'Q'_{vap}$, and $w'\Theta'$ are total quantities (sub-grid + advected). w'^2 is used as an indicator for circulation strength, whilst the total (advected plus sub-grid) water vapour and buoyancy fluxes illustrate the mean dynamical motions in the BL. A combined measure of sub-grid and advected fluxes are shown as these are of similar orders of magnitude and both make a non-negligible contribution to the flux budget (not shown, Fig. S7). In particular, the sub-grid $w'Q'_{vap}$ fluxes are dominant in cloud and near the surface, due to the stability of these layers. Area in grey represents CNTRL cloudy regions.

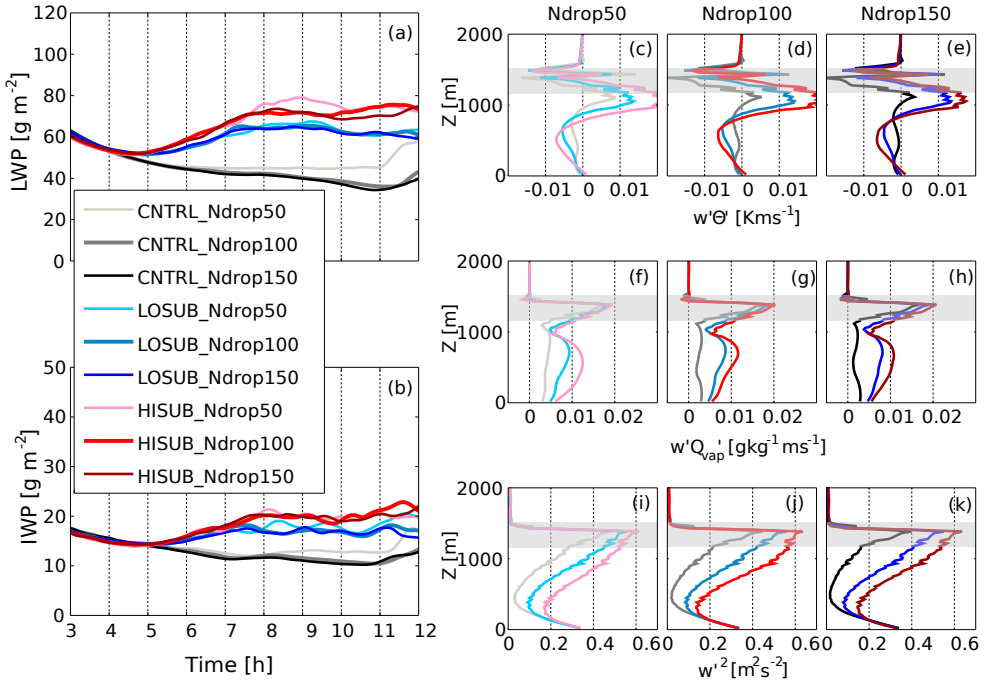

Figure 4. Domain-averaged LWP **(a)** and IWP **(b)** time series for simulations with different N_{drop} whilst varying the imposed W_{sub}. Black: control cases; blue: low W_{sub}; red: high W_{sub}. **(c–e)** buoyancy flux ($w'\Theta'$), **(f–h)** water vapour flux ($w'Q'_{vap}$), **(i–k)** vertical velocity variance (w'^2). Vertical profiles shown at 9 h.

Increasing N_{drop} has a smaller effect on N_{rain} than decreasing it, as expected by the thermodynamic indirect effect; with more droplets available, droplet size decreases due to less competition for water vapour. N_{rain} decreases in Ndrop150 with respect to the Ndrop100 or Ndrop50 cases, and the in-cloud mass production and below-cloud evaporation rates are smaller. Despite this, increasing W_{sub} still marginally increases the mass production/evaporation rates with respect to the CNTRL_Ndrop150 case.

From these simulations, we suggest that the level of imposed large-scale subsidence can significantly affect the liquid phase in clean mixed-phase Sc, as W_{sub} positively forces the rain mass production/evaporation rates modelled in these precipitation-favouring microphysical scenarios.

3.3 Test 3: ice number concentration

The influence of W_{sub} on a mixed-phase marine Sc when changing ice number concentrations is now considered. Heterogeneous primary ice formation is represented using the D10 parameterisation with aerosol number concentrations calculated during the study by Young et al. (2017). Previous studies (Harrington et al., 1999; Harrington and Olsson, 2001; Prenni et al., 2007; Morrison et al., 2012; de Boer et al., 2011; Young et al., 2017) have shown that the lifetime of springtime single-layer mixed-phase clouds at high latitudes is strongly dependent on N_{ice}. Here, a lower ($N_{ice} = \mathrm{D10} \times 0.5$) and higher ($N_{ice} = \mathrm{D10} \times 2$) threshold are implemented to change the number concentration of modelled ice, and snow, particles.

Figure 6 illustrates the domain-averaged LWP and IWP for test 3. The CNTRL cloud layer – as shown by the shaded area in Fig. 6c–k – becomes shallower with increasing N_{ice}. When no subsidence is imposed (CNTRL, black/grey lines Fig. 6a), decreasing N_{ice} increases the LWP as expected through the influence of the WBF mechanism, whereas increasing N_{ice} has the opposite effect. However, in CNTRL_D10x2, both the LWP and IWP increase sharply after 9 h (Fig. 6a, b). This LWP peak occurs earlier with increasing W_{sub} (as shown by the blue and brown traces in Fig. 6a). This trend can also be seen in the IWP traces. The cause of this increase is not clear; however, it may be due to localised cloud convection caused by the high N_{ice}, which has been previously modelled by Young et al. (2017).

Trios can be easily identified in Fig. 6a, where decreasing N_{ice} affects the LWP more so than altering W_{sub}. Although the key factor influencing the LWP is N_{ice}, W_{sub} acts to produce LWPs which are stable, or even increase, with time. In contrast, the CNTRL simulations typically produce a decreasing trend (with the exception of the D10 × 2 scenario).

W_{sub} affects the modelled fluxes (Fig. 6c–k) more so than altering N_{ice}; however, the exception to this trend is the high N_{ice} (D10 × 2) simulations, as subsidence does not stimulate this scenario as clearly as the other microphysical scenarios shown. Despite this, there are some notable differences in the

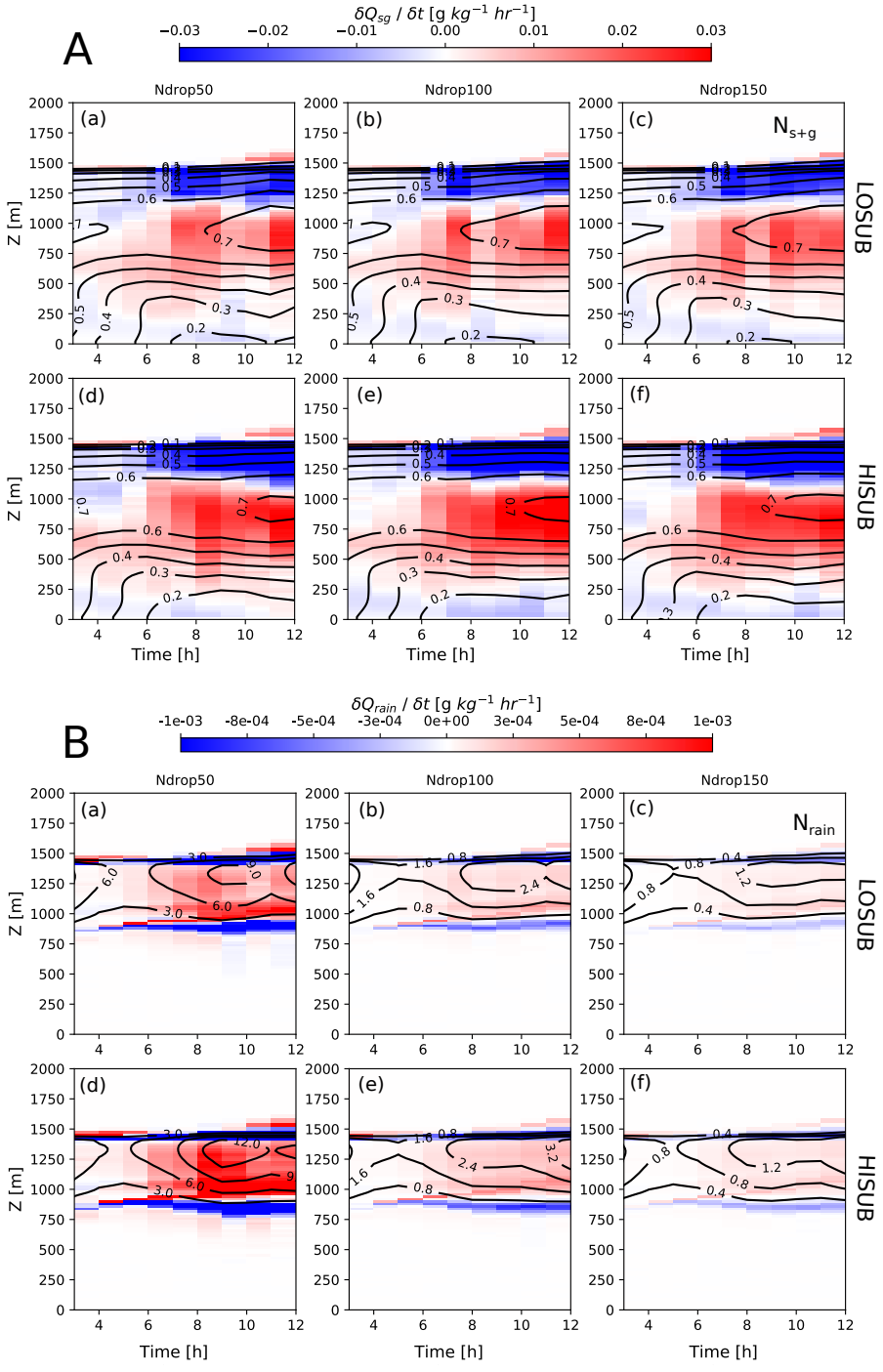

Figure 5. A: change in $\delta Q_{\mathrm{sg}}/\delta t$ ($\mathrm{g\,kg^{-1}\,h^{-1}}$) (shading) between subsidence cases and the corresponding CNTRL simulation for test 2. Red corresponds to increased production, whilst blue shows increased sublimation relative to the associated CNTRL. N_{sg} ($\mathrm{L^{-1}}$) is shown as contours. B: as panel A, instead the change in $\delta Q_{\mathrm{rain}}/\delta t$ ($\mathrm{g\,kg^{-1}\,h^{-1}}$) is shown with N_{rain} ($\mathrm{L^{-1}}$) as contours. **(a–c)** LOSUB, **(d–f)** HISUB.

flux profiles: for example, the extremes in the $w'\Theta'$ profiles are more exaggerated in the LO- and HISUB cases than the CNTRL when a lower N_{ice} is modelled (Fig. 6c–e). These comparisons suggest that W_{sub} can have a strong dynamical effect on liquid-dominated mixed-phase clouds, but its influence on those with more ice is limited.

From Fig. 7A, N_{sg} increases with increasing N_{ice} and decreases only slightly between the LO- and HISUB cases. Additionally, snow mass sublimation rates at cloud top and

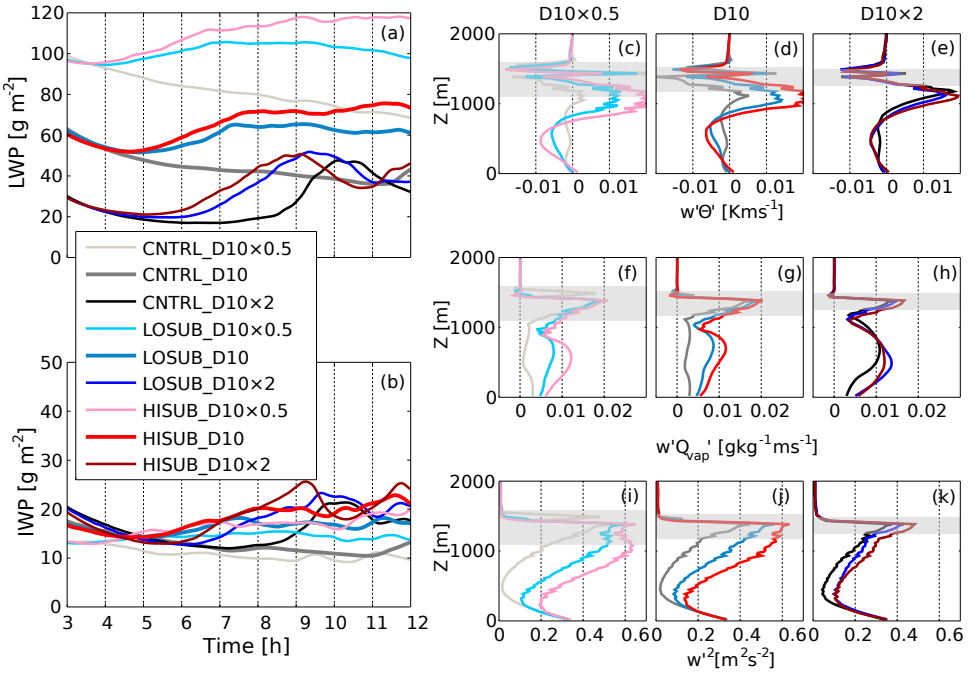

Figure 6. As Fig. 4 but with changing ice number concentrations.

production rates below cloud increase with increased W_{sub}. The increase in LWP and IWP in CNTRL_D10x2 at 9–10 h (Fig. 6a) affects our comparison, as increased snow mass is modelled at this time; therefore, the LO- and HISUB_D10x2 simulations produce less snow mass than the baseline.

Efficient rain mass production takes place with a lower N_{ice}, as shown in Fig. 7B, due to the greater liquid mass being distributed over a fixed N_{drop}. $\delta Q_{rain}/\delta t$ increases with W_{sub} in the D10 × 0.5 case. In-cloud mass production and below-cloud rain evaporation rates increase in LO- and HISUB_D10x0.5 relative to CNTRL_D10x0.5, as do the snow growth rates below cloud (Fig. 7B). With less ice available, cloud-top radiative cooling becomes more efficient due to a heightened liquid fraction (Fig. 6a), increased rain formation (Fig. 7Bd), efficient snow growth (Fig. 7Ad), and vigorous turbulence (Fig. 6i). Consequently, cloud-top height increases in D10 × 0.5, whilst this ascent is suppressed in D10 × 2. This ascent adds complexity into the interpretation of Fig. 7Aa, Ad, Ba, and Bd as we are comparing clouds which are ascending at different rates. Strong cloud-top evaporation/sublimation of rain/snow is modelled above 1500 m with the ascending CNTRL cloud, whilst the LO- and HISUB cases have no activity at these altitudes; therefore the anomaly between the W_{sub} and CNTRL simulations appears positive at these heights.

LWP and below-cloud rain evaporation are enhanced in CNTRL_D10x0.5 with comparison to CNTRL_D10 and CNTRL_D10x2; however, w'^2 is not strongly affected (Fig. 6i–k). Figure 8 shows $\delta Q_{sg}/\delta t$ and $\delta Q_{rain}/\delta t$ at 9 h to illustrate differences between the D10 × 0.5, D10, and D10 × 2 CNTRL cases. $\delta Q_{sg}/\delta t$ is similar in the D10 and D10x0.5 simulations, whilst the LWP and rain evaporation/production processes are positively forced by decreasing N_{ice}. In the turbulent subsidence cases, $\delta Q_{sg}/\delta t$ does increase below cloud with increasing W_{sub} (Fig. 7A). This is the only key difference between decreasing N_{ice} and increasing W_{sub}; therefore, increased latent heating through snow growth at cloud base – alongside heightened below-cloud rain evaporation and efficient cloud-top radiative cooling via a high LWP – is required to generate the heightened TKE (as illustrated here by w'^2) in these scenarios. Convection is suitably induced in LO- and HISUB_D10x0.5 as the modelled snow growth rates are greater (Fig. S8). Whilst the same N_{ice} is modelled in each of these scenarios, the subsidence cases produce a much colder BL than CNTRL_D10x0.5; therefore, the environmental conditions in LO- and HISUB_D10x0.5 facilitate snow growth below cloud, whilst the control produces comparatively inefficient growth conditions.

w'^2 is greatest with the LO- and HISUB_D10x0.5 simulations (Fig. 6i) due to dynamical stimulation by the heightened rain mass evaporation and snow mass production at cloud base (Fig. 7B). The clouds are more dynamic with increasing W_{sub}, and it is the liquid-dominated (D10x0.5) clouds which are more vulnerable to this dynamic stimulation. Clouds with greater N_{ice} suppress the liquid phase; therefore, N_{ice} has a key role in mediating the strength of turbulent overturning generated in the mixed-phase clouds.

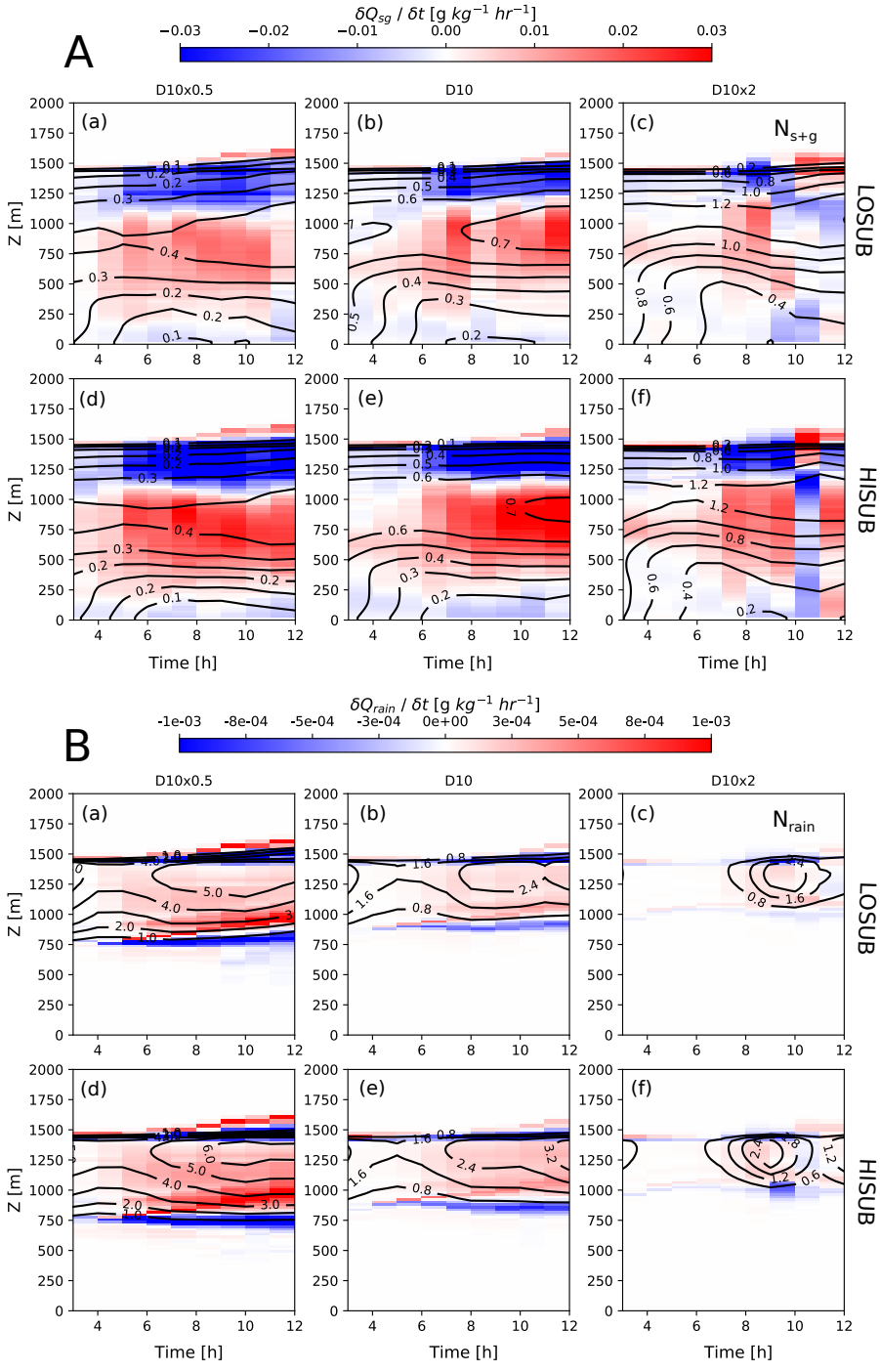

Figure 7. As Fig. 5, but instead the ice number concentration is varied (test 3).

3.4 Test 4: surface warming

As described in Sect. 2, our previous tests consider scenarios that would elicit a microphysical response whilst keeping the surface boundary conditions approximately constant. Tests 1–3 are idealised and are not representative of the environmental forcings encountered when these clouds move southwards: observations show a sharp near-surface air temperature gradient in CAO flows transitioning southwards from the cold sea ice to the warm ocean. To address this, we further consider the combined dynamical impact of large-scale subsidence and a warming surface on both the BL and cloud microphysical structure. Whilst our domain size is not appro-

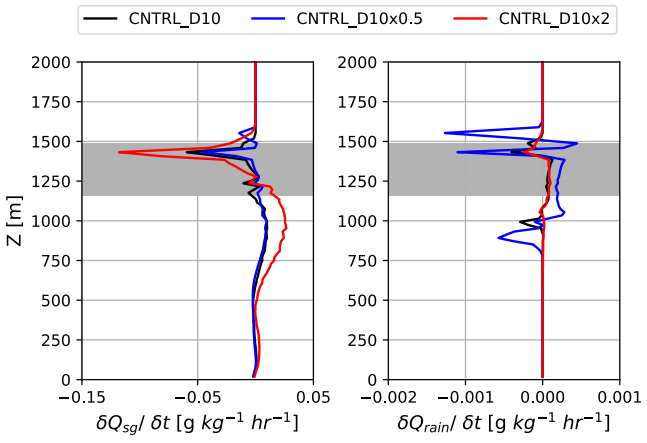

Figure 8. Microphysical tendencies comparison of CNTRL_D10, CNTRL_D10x0.5, and CNTRL_D10x2. Vertical profiles, at 9 h, of solid precipitation (snow + graupel) mass tendency ($\delta Q_{\mathrm{sg}}/\delta t$) and rain mass tendency ($\delta Q_{\mathrm{rain}}/\delta t$) are shown. Area in grey represents CNTRL_D10 cloudy regions.

priate to resolve the explicit transition from closed- to open-cellular convection far downstream in a CAO, we will show how large-scale subsidence influences the microphysical stability of a stable mixed-phase marine Sc over a warming surface, upstream from this strong cellular convection.

More convection is modelled with time under the destabilising conditions of a warming surface (Fig. 9). Domain-averaged LWPs and IWPs are similar in the subsidence cases, increasing almost monotonically with time (Fig. 9a, b). Slightly greater LWPs are modelled in HISUB_SURFWARM than in the LOSUB counterpart. Subsidence acts to produce greater LWPs and IWPs than the CNTRL up to approximately 10 h, at which point CNTRL_SURFWARM undergoes a significant convective transformation marked by a sharp increase in both LWP and IWP. Planar views of Fig. 9c–e show that, at this time, the CNTRL_ SURFWARM cloud contains numerous regions of very high LWP ($> 200\,\mathrm{g\,m^{-2}}$) and IWP ($> 50\,\mathrm{g\,m^{-2}}$) co-located with strong updraughts at 1000 m.

Cloud top and surface sources of TKE couple in all cases (Fig. 10a–c). The CNTRL case couples rapidly at approximately 10 h (Fig. 10a), coincident with the peak in LWP and IWP shown in Fig. 9a, b. Within approximately 1.5 h, the two TKE sources decouple again. Cloud top and surface sources of TKE dominate the LO- and HISUB_SURFWARM profiles separately from approximately 7 h onwards. LOSUB_SURFWARM displays a similar coupling at 10 h to CNTRL_SURFWARM, yet it remains coupled afterwards and undergoes a second TKE burst between 11 and 12 h. TKE evolution in HISUB_SURFWARM is more gradual than the CNTRL and LOSUB cases: the top-down and bottom-up propagation of TKE steadily increases with time to couple the separated cloud and surface sources.

Cloud-top height increases in CNTRL_SURFWARM (Fig. 10a), whilst this ascent is strongly suppressed in HISUB_SURFWARM (Fig. 10c) and marginally suppressed in LOSUB_SURFWARM (Fig. 10b). Negative $w'\Theta'$ fluxes at cloud top again suggest entrainment of warm air into the cloud layer from above the BL in each case; however, this flux is stronger in CNTRL_SURFWARM than in the subsidence cases, indicating that greater entrainment rates are accompanying the cloud-top ascent.

Significantly larger values of $w'Q'_{\mathrm{vap}}$ and $w'\Theta'$ are modelled below cloud in the CNTRL_SURFWARM simulation ($0.052\,\mathrm{g\,kg^{-1}\,m\,s^{-1}}$ and $0.045\,\mathrm{K\,m\,s^{-1}}$, respectively) than in the subsidence cases, coinciding with the rapid BL coupling shown in Fig. 10a. Convective activity increases at this time, with w'^2 increasing up to $0.90\,\mathrm{m^2\,s^{-2}}$ in cloud alongside a peak (cloud top) TKE of $2.8\,\mathrm{m^2\,s^{-2}}$ (Table 3). Additionally, rain mass production is enhanced in CNTRL_SURFWARM; however, below-cloud rain evaporation is still weaker than in the LO- and HISUB_SURFWARM simulations. Rain evaporative cooling below cloud in LO- and HISUB_SURFWARM acts to decouple the surface and in-cloud heat sources from each other (Fig. 10i). As a result, the $w'\Theta'$ profiles swing through significant extremes below cloud: from 0.021, through -0.011, to $0.028\,\mathrm{K\,m\,s^{-1}}$ in the HISUB_SURFWARM case. Furthermore, the warming surface produces an unstable Θ_{il} profile at the surface in each simulation (Fig. 10f).

Z–X slices of several microphysical variables from CNTRL_SURFWARM are shown in Fig. 11 to illustrate the cloud structure at 10 h. In the bottom panel, below-cloud cumuli form which either couple to the Sc layer (white ellipses) or remain separate (red ellipses). Cumuli are identified by adjacent updraught/downdraught regions with 100 % relative humidity (or close to 100 %). These cumuli structures are clearly visible in the Q_{liq} contour field (top panel, Fig. 11). Cumuli can be seen from 8 h onwards and become more frequent with time. At this time, two spatially close cumuli form at approximately -7000 and -3500 m, marking the boundaries of a detraining layer of moisture above cloud top. Additionally, a similar, completely detached moist layer can be seen above cloud top coinciding with the 6000 m cumulus.

HISUB_SURFWARM has much larger updraught and downdraught regions than CNTRL_SURFWARM: from approximately 11 h onwards, these often extend to almost the full height of the BL (Fig. 12). No distinct sub-cloud cumuli can be identified in HISUB_SURFWARM, whereas these are common in CNTRL_SURFWARM (Fig. 11): the addition of subsidence acts to suppress their formation and allow a more homogeneous Sc layer to be maintained in a BL undergoing top-down and bottom-up coupling of TKE. The coupling process is more gradual in HISUB_SURFWARM than the CNTRL or LOSUB counterparts, suggesting that subsidence plays a role in whether or not this rapid TKE coupling and cloud-top ascent can take place.

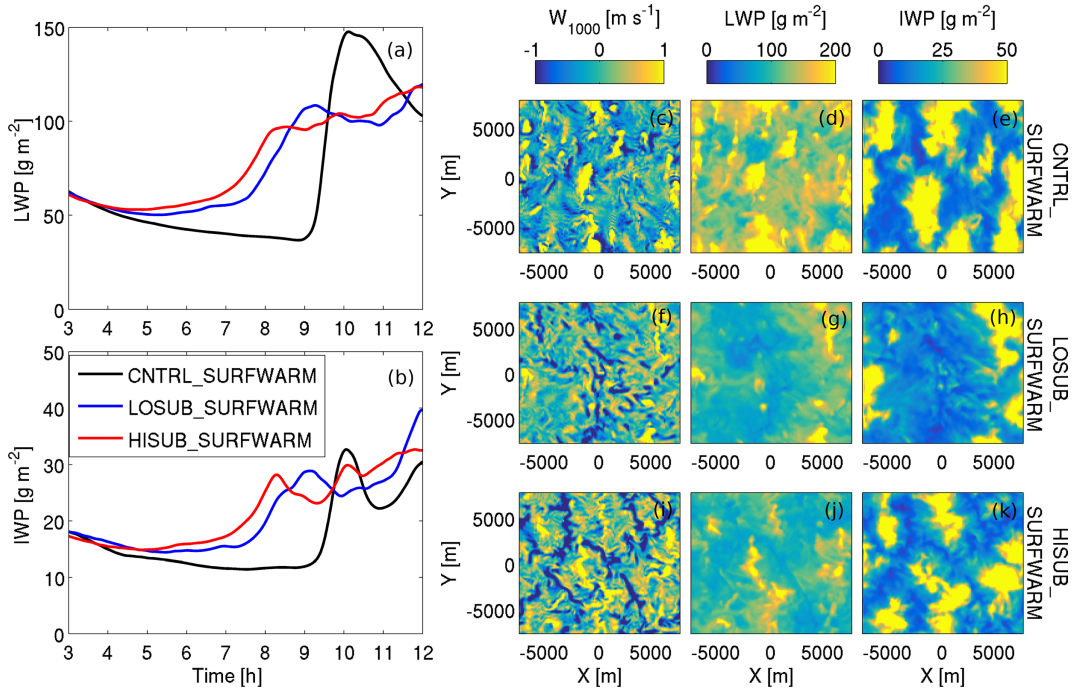

Figure 9. As Fig. 2 but with the addition of a warming surface (test 4). Planar views **(c–k)** are shown at 10 h to capture the bulk cloud structure coinciding with the CNTRL_SURFWARM peak in LWP and IWP shown in panels **(a)** and **(b)**.

Table 3. Key BL and cloud microphysical parameters affected by large-scale subsidence in test 4. Mass tendencies are quoted at 10 h, comparable with Fig. 10.

Run label	Peak TKE[a,b] [$m^2\ s^{-2}$]	$\Delta\Theta_{il}$ [K]	Peak LWP[b] [$g\ m^{-2}$]	Peak IWP[b] [$g\ m^{-2}$]	Min/Max $\delta Q_{sg}/\delta t$ [$g\ kg^{-1}\ h^{-1}$]	Min[c]/Max $\delta Q_{rain}/\delta t$ [$g\ kg^{-1}\ h^{-1}$]
CNTRL	2.8	7.63	147.7	32.7	−0.266/0.083	$-4.8\times10^{-4}/1.8\times10^{-3}$
LOSUB	3.9	8.06	119.8	39.6	−0.234/0.051	$-1.3\times10^{-3}/4.5\times10^{-4}$
HISUB	2.3	8.37	118.3	32.7	−0.284/0.071	$-1.3\times10^{-3}/6.6\times10^{-4}$

[a] At cloud top. [b] Maximum values attained within 12 h simulation time. [c] Minimum below cloud.

4 Discussion

4.1 Effect of subsidence on bulk cloud properties

Imposing large-scale subsidence in simulations of marine Arctic mixed-phase Sc increases the LWP and IWP of the modelled clouds through increased convective activity throughout the domain (Fig. 2). W_{sub} does not affect the cloud depth (Figs. 5, 7); only N_{ice} notably affects the modelled cloud depth (Fig. 6). Dynamical stimulation by subsidence – which would sustain a mixed-phase Sc for longer against the WBF mechanism – may therefore have been previously missed in observations and modelling studies. Increasing W_{sub} has a greater effect on the liquid phase than the ice phase (Figs. 2, 4, 6); however, increasing subsidence causes the development of heterogeneity in the LWP and IWP fields, leading to instabilities in the modelled clouds. In particular, the radiative properties of the clouds would be affected by the heterogeneous spread in LWP, where regions of high LWP would be more reflective to incoming SW radiation (Schröter et al., 2005) and more efficiently cooled via longwave radiative cooling.

Localised regions of high IWP are typically co-located with updraughts in our simulations, likely due to the method of parameterising ice nucleation in our model. Namely, additional nucleation mechanisms (e.g. contact, immersion) are not represented to give us a predictable source of ice number concentrations (similar to Young et al., 2017). These mechanisms would likely influence our results if they were explicitly resolved in our model; for example, we would expect contact nucleation in downdraughts, through interaction with interstitial aerosol particles.

Subsidence strongly influences the LWP; however, increasing W_{sub} marginally increases the domain-averaged IWP (Fig. 2b). Figure 6b shows that the peak IWP attained

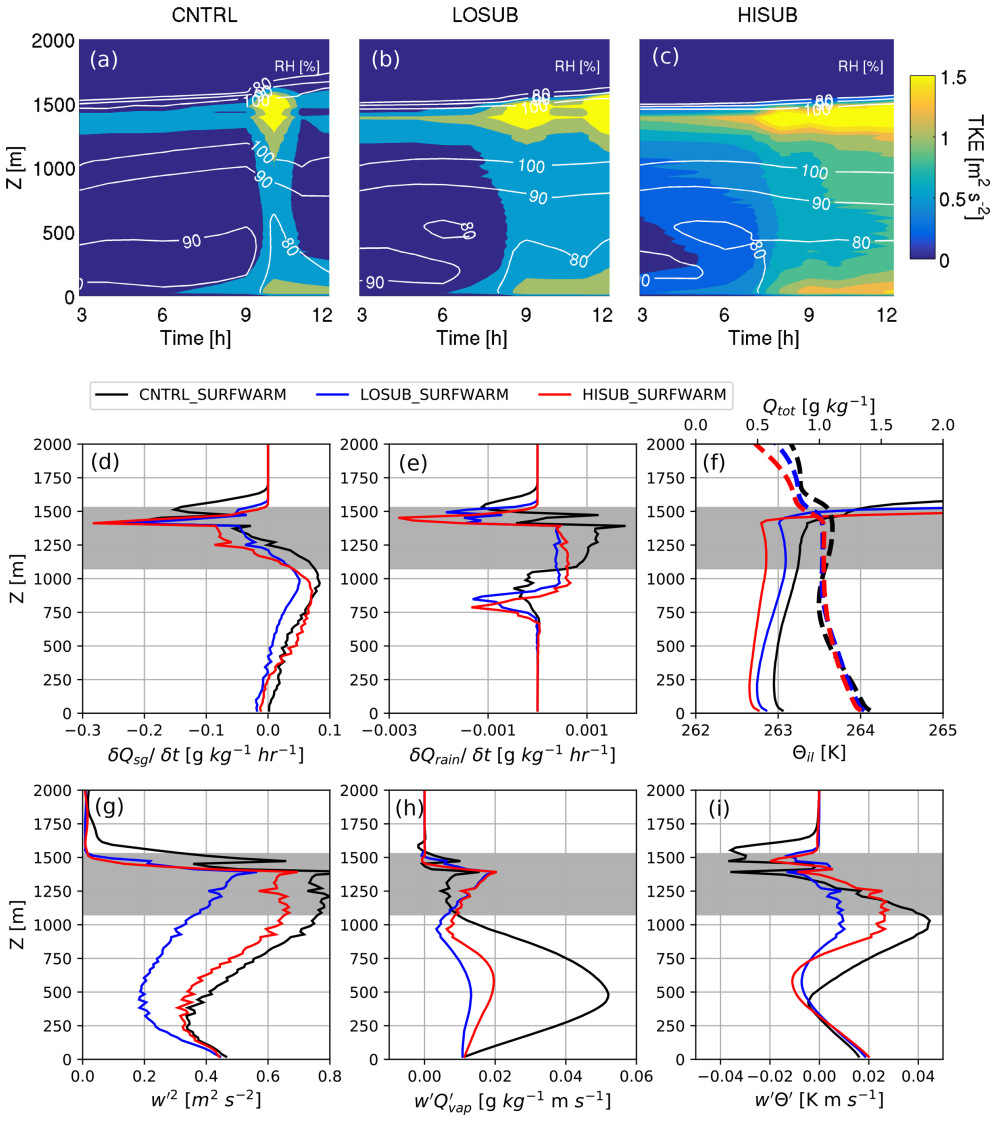

Figure 10. As Fig. 3 but with the addition of a warming surface (test 4). Note the different colour scale in panels **(a)–(c)** and extended x range over which data are shown in all panels except **(f)**, with comparison to Fig. 3. Vertical profiles (panels **d–i**) are shown at 10 h.

by CNTRL_D10x2 is also achieved in the HISUB_D10 case, suggesting that increasing W_{sub} can have a similar effect on the bulk ice properties of the cloud as increasing N_{ice}. However, a much larger LWP is also modelled when subsidence is imposed, creating a microphysical structure that may be more robust against the WBF mechanism. This may allow mixed-phase conditions to be sustained for longer against a higher N_{ice} – a problem that is often faced when modelling Arctic mixed-phase Sc (Harrington and Olsson, 2001; Prenni et al., 2007; Morrison et al., 2012; de Boer et al., 2011, 2014; Young et al., 2017).

4.2 Effect of subsidence on microphysics and precipitation

In the chosen microphysical scenarios that may affect precipitation development in mixed-phase marine Sc, W_{sub} enhances rain evaporation at cloud top and base. Increased subsidence leads to larger rain mass production rates and a greater N_{rain} within cloud, and this effect is particularly clear when lowering either N_{drop} (Ndrop50, Fig. 5) or N_{ice} (D10 × 0.5, Fig. 7). In these cases, the increase in N_{rain} due to subsidence is less than can be attributed to the microphysical changes; for example, an increase of approximately 6 L^{-1} is modelled in the Ndrop50 scenario due to increasing W_{sub}, whilst an increase of approximately 9 L^{-1} is achieved by lowering N_{drop} from 100 to 50 cm^{-3} (Fig. 5B).

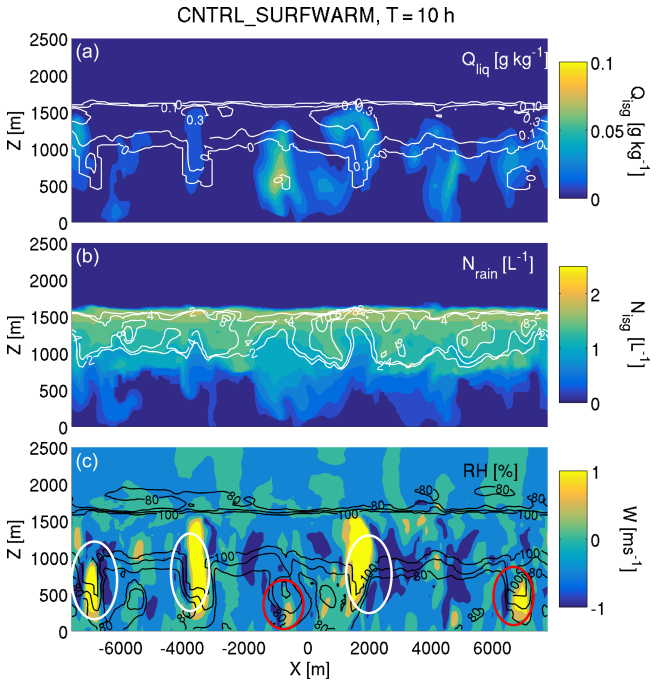

Figure 11. Z–X slices for the CNTRL_SURFWARM case at 10 h. **(a)** Total ice mass mixing ratio (Q_{isg}, shading) and liquid water mass mixing ratio (Q_{liq}, contours). **(b)** Total ice number concentration (ice + snow + graupel, N_{isg}, shading) and rain number concentration (N_{rain}, contours). **(c)** Vertical velocity (W, shading) and relative humidity (RH, contours). Identified detached below-cloud cumuli are highlighted by red ellipses, and cumuli merged with the Sc are indicated by white ellipses.

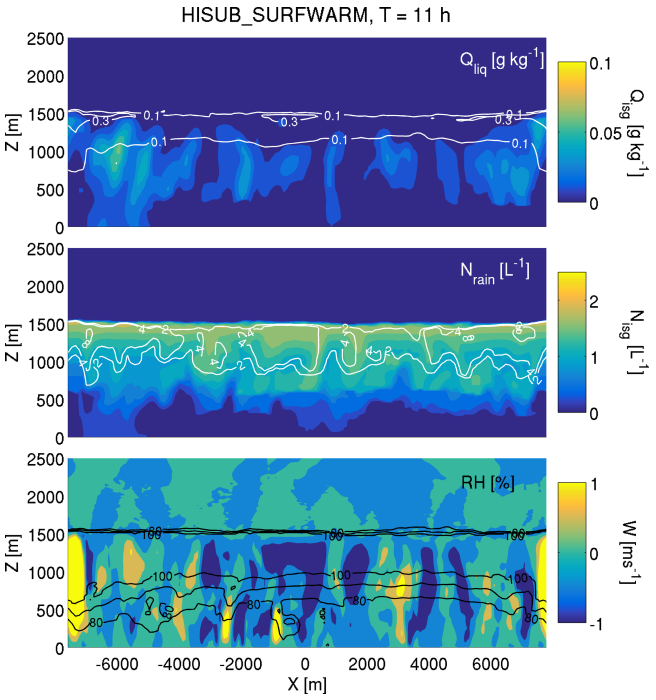

Figure 12. Z–X slices for the HISUB_SURFWARM case at 12 h. Panels are arranged similarly to Fig. 11.

From tests 2 and 3, W_{sub} amplifies the modelled turbulence in scenarios allowing for efficient rain formation (e.g. Ndrop50, Fig 4i). W_{sub} also acts to promote more turbulence (Fig. 4k) and rain formation (Fig. 5B) in a microphysical scenario that produces little rain in its absence (Ndrop150). Conversely, increasing N_{ice} in test 3 does not have the same effect, and W_{sub} does little to promote turbulence in this scenario. Whilst the ice categories do little to stimulate convection, they are responsible for suppressing rain formation; for example, a higher N_{ice} (and thus, N_{sg}) suppresses the strong rain production/evaporation processes modelled at a lower N_{ice} (Fig. 7B). With weakened rain formation and evaporation, less vigorous overturning is modelled in D10 × 2 than D10 or D10 × 0.5. Whilst the liquid phase drives the development of dynamical overturning, the ice phase has a strong influence – through the WBF mechanism – on whether this convective activity can actually develop.

Similarly, total ice number concentrations (ice + snow + graupel, N_{isg}, Fig. 11b) are largely unaffected by a warming surface (with comparison to Fig. S3b); however, both Q_{liq} and N_{rain} increase. Precipitation formation is enhanced in downdraught regions (Figs. 11, 12). Weaker below-cloud rain evaporation occurs in CNTRL_SURFWARM (Fig. 10e), and the upward propagation of heat and moisture from the surface causes distinct cumuli to form below cloud and join with cloud base. These cumuli dynamically stimulate the cloud from below (Fig. 11) and have a similar effect on the cloud as the introduction of subsidence in tests 1–3; for example, the warming surface allows a greater N_{rain} to form in cloud (Fig. 11). In fact, N_{rain} in CNTRL_SURFWARM is much more comparable with the corresponding domain-averaged values of the LO- and HISUB_Ndrop50 simulations in test 2 (Fig. 5B) – the efficient-liquid-precipitation cases – than any of the previous control simulations.

These findings indicate that subsidence has the potential to positively force the liquid phase in Arctic mixed-phase marine Sc whilst having little effect on the ice phase. Young et al. (2016) presented observations of cloud microphysics over the transition from sea ice to ocean and found that the ice phase changed little under the dynamical evolution of the BL, whilst the liquid water content increased four-fold. Therefore, mixed-phase clouds with low number concentrations of primary ice, such as those commonly observed in the springtime Arctic, may be vulnerable to dynamical changes induced by subsiding air from above or a warming surface from below.

4.3 Effect of subsidence on the BL and dynamics

In tests 1–3, convective activity increases with W_{sub} through increased BL TKE and below-cloud w'^2. Solar heating acts

to marginally offset the formation of defined closed-cellular structure; however, the cloud-driven convection is strongly dependent on cloud-top LW radiative cooling (see Fig. S6). Additionally, rain mass formation rates, number concentrations, and the domain-averaged LWP increase with increasing W_{sub}. This finding mirrors the conclusions of Hill et al. (2014), where the authors found that increasing the resolved TKE and/or temperature positively influences the liquid phase in an ice-saturated environment, as these conditions contribute towards sustaining water saturation.

In the absence of surface warming, all modelled BLs display a stable Θ_{il} profile. This stability is likely influenced by the stable conditions used to initialise the model, and one must note that only a single set of initial conditions were used in this study. A moist layer is maintained close to the surface in the CNTRL simulation (Fig. 3a), below the sub-cloud mixed layer, whereas this moisture source is eroded in the subsidence cases. Additionally, the CNTRL case presents a minor BL Θ_{il} inversion, and a stronger Q_{tot} inversion, at approximately 500 m. The combination of these inversions and the moist surface layer suggests that the CNTRL simulation is, in fact, more strongly decoupled from the surface than the subsidence cases at the time step shown (9 h, Fig. 3). However, the subsidence cases display a similar strongly decoupled profile in TKE to the CNTRL at earlier times (e.g. 5 h, Fig. 3). TKE increases with time in the BL when subsidence is imposed, and it promotes top-down mixing of TKE through the sub-cloud layer towards the surface by the end of the simulations, tending towards a coupled profile. However, cloud-top TKE still dominates the BL profiles in the LO- and HISUB cases (Fig. 3b, c), suggesting that mixing throughout the BL is still not homogeneous and the clouds remain approximately decoupled from the surface by the termination time of the simulations. This decoupling allows radiative cooling at cloud top and evaporative cooling/latent heating below cloud to drive convective activity in the cloud layers, irrespective of surface sources.

With a larger LWP, stronger cloud-top radiative cooling is expected, promoting a greater cloud-top height (Wang and Feingold, 2009a). Subsidence acts to restrict cloud-top ascent by reinforcing the BL temperature inversion (Table 2), thus lowering the entrainment rate of air from above. Cloud LWP increases in the absence of notable entrainment, allowing for stronger cloud-top LW radiative cooling and subsequent precipitation development within cloud. BL temperatures are therefore cooler with imposed subsidence than without (Fig. 3i), due to the combined effect of reduced entrainment, strong cloud-top radiative cooling, and enhanced evaporative cooling below cloud.

A lack of subsidence combined with a warming surface acts to push cloud top significantly higher, and increase the LWP, through the formation of the below-cloud cumuli (namely in CNTRL and LOSUB_SURFWARM, Fig. 9d). Higher levels of W_{sub} act to stabilise the Sc layer and suppress cumuli formation from the warming surface (as is seen in the CNTRL_SURFWARM case). TKE production is positively influenced in the CNTRL and LOSUB_SURFWARM cases, with strongly separated cloud and surface sources, and peak values approximately 3 times greater than modelled in test 1 (Tables 2 and 3). Cloud-top TKE splits in two in both CNTRL and LOSUB_SURFWARM (Fig. 10a, b); however, it is unlikely that this is a domain artefact as the vertical resolution is consistent through this altitude range. It is possible that the PW advection scheme is introducing spurious oscillations into the advected quantities, caused by the the sharp gradient at the cloud boundary due to the formation of these dynamic cumuli (as discussed by Gray et al., 2001). Peak TKE is only marginally stronger in HISUB_SURFWARM than in test 1 (Tables 2 and 3), suggesting that higher W_{sub} offsets the efficient in-cloud TKE production which occurs when the system is additionally forced by a warming surface. By suppressing the formation of below-cloud cumuli, subsidence acts to produce a stable, yet dynamic, Sc layer, whilst strong convection and spatial heterogeneity are simulated with low or no subsidence. With more heterogeneity, there is an increased likelihood for instability in the cloud layer, which will likely influence the fate of the cloud downstream.

4.4 Role of domain resolution

Whilst CAOs are discussed to motivate our study, we must stress that our chosen domain configuration is not optimal for the explicit study of Sc-to-cumulus transitions downstream in a CAO. Large high-resolution domains are required to accurately resolve the small-scale microphysical processes within these phenomena (Field et al., 2014); however, our domain size and resolution are restricted by computational expense. Bretherton et al. (1999) demonstrated that our spatial resolution may allow entrainment rates to be overpredicted by approximately 50 % (Connolly et al., 2013). Whilst the authors concluded that the resolution imposed here can still provide a useful insight into BL evolution, accurately resolved turbulence requires higher spatial resolution. Feingold et al. (2015) found that a higher-resolution set-up produced enhanced BL convection and a deeper BL depth. Furthermore, Wang and Feingold (2009a) found that the simulated vertical mixing of vapour and Θ fields improved, and the modelled LWP increased, in their open-cellular convection simulations by increasing spatial resolution.

To test the influence of resolution on our findings, we increase the horizontal resolution to 60 m (Δx) and the vertical resolution to 10 m, whilst maintaining the domain height. This set-up therefore decreases the spatial extent of the domain by half in both X and Y. Vertical resolution was 10 m up to 2000 m, decreasing to 20 m above this height. By increasing our model resolution, we aim to provide a more accurate representation of the modelled entrainment rates. Due to computational expense, only two test cases are considered: the CNTRL and HISUB simulations from test 1 (Sect. 3.1).

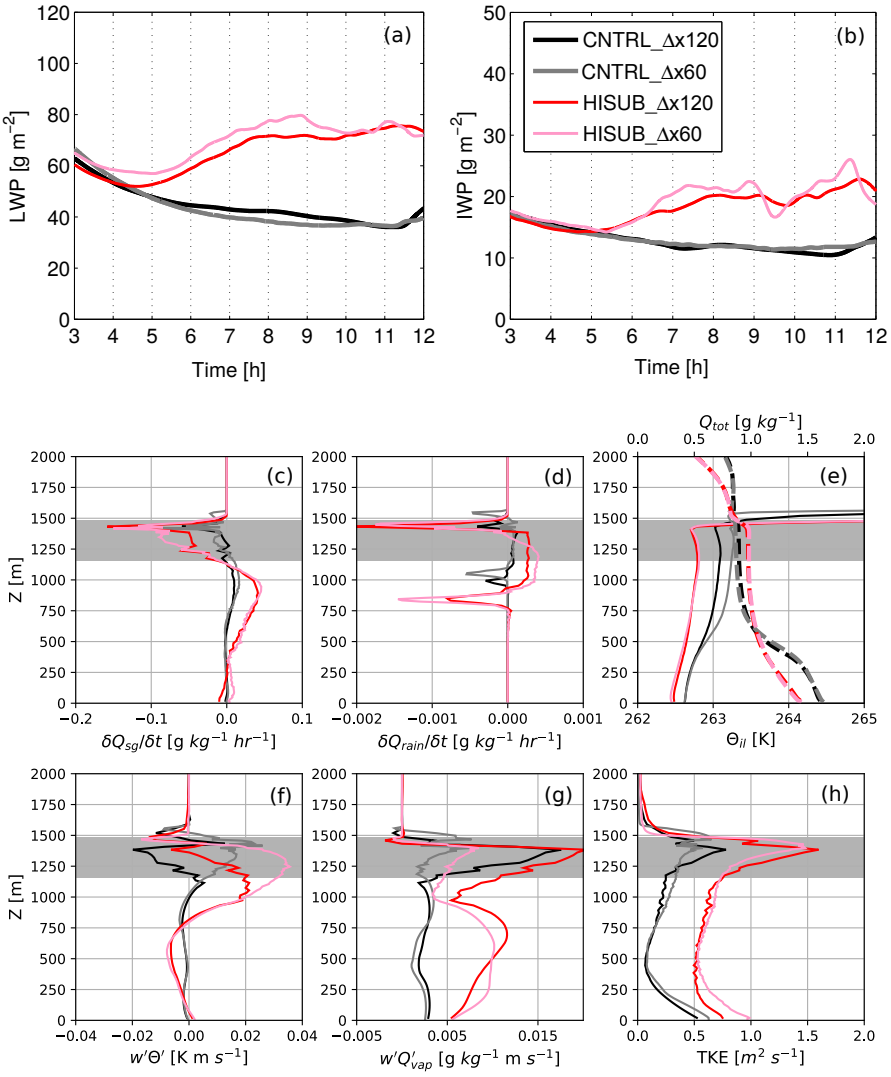

Figure 13. Influence of domain resolution on changing imposed large-scale subsidence. Only the CNTRL and HISUB cases are considered. LWP **(a)** and IWP **(b)** time series for simulations with 120 m resolution (default configuration) and 60 m resolution (high-resolution configuration). Black: CNTRL, default; grey: CNTRL, high resolution; red: HISUB, default; and pink: HISUB, high resolution. **(c–h)** Vertical profiles (at 9 h) of **(c)** solid precipitation (snow + graupel) mass tendency ($\delta Q_{\mathrm{sg}}/\delta t$), **(d)** rain mass tendency ($\delta Q_{\mathrm{rain}}/\delta t$), **(e)** ice–liquid potential temperature (Θ_{il}, solid) and total water mixing ratio (Q_{tot}, dashed), **(f)** buoyancy flux ($w'\Theta'$), **(g)** vertical flux of water vapour ($w'Q'_{\mathrm{vap}}$), and **(h)** total turbulent kinetic energy (TKE). Fluxes shown are total quantities (sub-grid + advected). Area in grey represents CNTRL_Δx120m cloudy regions.

Little difference between the domain-averaged LWP and IWP can be identified between the CNTRL cases (black/grey, Fig. 13a, b). In the HISUB example, increasing the model resolution amplifies the irregularities in both the LWP and IWP traces. In particular, the IWP is significantly more variable with time than in the default set-up.

In general, increasing the resolution does not alter the trends identified previously – for example, the positive below-cloud moisture fluxes, higher below-cloud rain mass evaporation and snow mass growth rates, and increased TKE with increasing W_{sub}. In fact, it should be noted that the below-cloud rain mass evaporation rates are enhanced with comparison to the coarse-resolution HISUB case, suggesting that the evaporation rates shown in Sect. 3.2, 3.3, and 3.4 may be underestimated. The Q_{tot} profiles illustrate clear decoupling in the CNTRLs, with a weaker inversion in the HISUB cases. Additionally, both $\Delta x60$ simulations produce a greater TKE peak towards the surface, in addition to the peak simulated at cloud top, due to the dominating influence of the subgrid contribution to the TKE towards the surface (Fig. 13h).

Whilst we can test the influence of increased resolution on our findings, increasing our domain size would be too computationally expensive for our set-up. Larger domains are often used to allow mesoscale interactions between developing open convective cells to be resolved. Schröter et al. (2005) suggest that a domain of 100×100 km, with 50–100 m spatial resolution, is required to truly encapsulate any mesoscale interactions between developing convective cells in CAOs. We cannot speculate what mesoscale interactions may occur between the different scenarios presented here; however, one must note that such interactions have been previously simulated to occur over the transition between closed and open convective cells in CAOs; thus these effects should be investigated in further work.

5 Conclusions

Large-scale subsidence is often imposed in LES models as a tuning factor to maintain cloud-top height; however, the influence of this parameter on mixed-phase cloud microphysics has not been previously investigated. Here, we have shown how large-scale subsidence affects the microphysical structure of Arctic mixed-phase marine Sc using the UK Met Office Large Eddy Model (Gray et al., 2001). By subjecting four idealised scenarios – a stable Sc, varied droplet (N_{drop}) or ice (N_{ice}) number concentrations, and a warming surface – to different levels of subsidence, we have identified a clear relationship between subsidence and convection development, with potential implications for mixed-phase BL clouds forming in the ocean-exposed Arctic regions.

Key features identified in this study are as follows:

- With no surface forcing (tests 1–3), increasing the imposed large-scale subsidence (W_{sub}) reinforces the BL temperature inversion and thus reduces entrainment from the free troposphere. With less air from aloft mixing into the clouds, a greater LWP (and often, IWP) develops, allowing for efficient precipitation development, cloud-top radiative cooling, and downdraught production. All of the rain produced evaporates below cloud. The combination of strong cloud-top radiative cooling, below-cloud rain evaporative cooling, and latent heating from snow growth at cloud base generates more TKE within the BL. These three requirements combine to form a feedback loop consisting of LWP, below-cloud rain evaporation/snow growth, and TKE development, positively forced by the magnitude of W_{sub}.

- In microphysical scenarios which promote efficient rain production (low N_{drop} or low N_{ice}), W_{sub} enhances rain mass production and evaporation rates, TKE at cloud top and at the surface, and turbulent activity throughout the BL. Modelled N_{rain} increases with W_{sub}, whilst N_{sg} marginally decreases. Modelled rain evaporates efficiently, coinciding with regions of snow growth. These microphysical processes stimulate the cloud dynamically by introducing perturbations in moisture and temperature below cloud. Only precipitation as snow reaches the surface, mirroring observations of mixed-phase marine Sc in the Arctic and in CAOs.

- Altering the ice phase feeds back onto the liquid phase through the influence of the WBF mechanism (test 3, Fig. 6). N_{ice} has a key role in mediating the strength of turbulent overturning induced in these mixed-phase clouds by suppressing the liquid phase. However, N_{ice} is also a crucial component at the opposite end of the scale: there needs to be enough ice present to produce enough latent heating via depositional growth to force convection from cloud base. With more dynamical motion, the liquid phase may be sustained more effectively against the WBF mechanism. This is a crucial result for the understanding of mixed-phase Sc in the Arctic – particularly in the Arctic spring – where high-pressure, stable conditions are common across the region. These clouds have been observed to persist for long periods of time, and subsidence caused by large-scale meteorology could be acting to sustain these clouds microphysically against dissipation or glaciation.

- The feedbacks identified from test 1–3 are not so clearly related when a warming surface is additionally imposed: significantly larger values of $w'Q'_{\mathrm{vap}}$ and $w'\Theta'$ are modelled with no W_{sub}, coinciding with the rapid BL coupling shown in Fig. 10a. In-cloud rain production rates produced in CNTRL_SURFWARM are also much greater than without surface forcing in test 1. A warming surface, with a lack of subsidence, acts to dynamically stimulate the modelled cloud from below, similar to how subsidence stimulates it from above. Below-cloud cumuli form in CNTRL_SURFWARM, and to a lesser extent in LOSUB_SURFWARM, which act to push cloud top higher, generate high LWPs, and cause significant spatial heterogeneity in the cloud layer. This cumuli formation is suppressed when under high levels of subsidence (HISUB_SURFWARM); the combination of these two forcings counteract one another to produce a stable, yet dynamic, Sc layer.

This study presents a clear relationship between large-scale subsidence and the development of convection in liquid-dominated mixed-phase clouds common to the Arctic. We propose that the influence of large-scale subsidence in both Arctic mixed-phase marine Sc and CAOs should be considered in further work, using models of different spatial scales. In particular, it would be beneficial to study the development of CAO flows – with a high-resolution, large domain – under a transitional profile of subsidence, i.e. flowing from a high-pressure region. Our results suggest that a high W_{sub} will amplify turbulent activity and rain production/evaporation in any stable mixed-phase Sc modelled, and

a weakening of subsidence alongside a warming surface will likely promote cloud-top ascent, below-cloud cumuli formation, and strong spatial heterogeneities throughout the cloud layer. Therefore, further investigating the role of subsidence in CAO flows will be beneficial to our ability to accurately model and understand the break-up of these cloud decks. More generally, comprehending the physical impact of subsidence on marine mixed-phase cloud microphysics at higher latitudes will allow us to better predict how clouds in the Arctic region may change in the depleted-sea-ice future.

Code availability. Please contact the UK Met Office for LEM code requests.

Data availability. LEM model runs are archived at the University of Manchester and are available on request.

The Supplement related to this article is available online at https://doi.org/10.5194/acp-18-1475-2018-supplement.

Competing interests. The authors declare that they have no conflict of interest.

Special issue statement. This article is part of the special issue "Aerosol-Cloud Coupling And Climate Interactions in the Arctic (ACCACIA) (ACP/BG inter-journal SI)". It is not affiliated with a conference.

Acknowledgements. Gillian Young was funded by the National Environment Research Council (NERC) as part of the ACCACIA campaign (grant NE/I028696/1). Paul J. Connolly acknowledges funding from EU FP7 project BACCHUS (grant agreement no. 603445). The authors are also grateful to Adrian Hill for his support with operating the LEM and to Martin Gallagher, Jonathan Crosier, and Keith Bower for helpful discussions throughout the duration of the study.

Edited by: Martina Krämer
Reviewed by: two anonymous referees

References

Abel, S. J., Boutle, I. A., Waite, K., Fox, S., Brown, P. R., Cotton, R., Lloyd, G., Choularton, T. W., and Bower, K. N.: The Role of Precipitation in Controlling the Transition from Stratocumulus to Cumulus Clouds in a Northern Hemisphere Cold-Air Outbreak, J. Atmos. Sci., 74, 2293–2314, https://doi.org/10.1175/JAS-D-16-0362.1, 2017.

Bodas-Salcedo, A., Williams, K. D., Field, P. R., and Lock, A. P.: The Surface Downwelling Solar Radiation Surplus over the Southern Ocean in the Met Office Model: The Role of Midlatitude Cyclone Clouds, J. Climate, 25, 7467–7486, https://doi.org/10.1175/JCLI-D-11-00702.1, 2012.

Bretherton, C. S., Macvean, M. K., Bechtold, P., Chlond, A., Cotton, W. R., Cuxart, J., Cuijpers, H., Mhairoutdinov, M., Kosovic, B., Lewellen, D., Moeng, C.-H., Siebesma, P., Stevens, B., Stevens, D. E., Sykes, I., and Wyant, M. C.: An intercomparison of radiatively driven entrainment and turbulence in a smoke cloud, as simulated by different numerical models, Q. J. Roy. Meteor. Soc., 125, 391–423, https://doi.org/10.1002/qj.49712555402, 1999.

Bryan, G. H. and Fritsch, J. M.: A Reevaluation of Ice-Liquid Water Potential Temperature, Mon. Weather Rev., 132, 2421–2431, https://doi.org/10.1175/1520-0493(2004)132<2421:AROIWP>2.0.CO;2, 2004.

Connolly, P. J., Vaughan, G., Cook, P., Allen, G., Coe, H., Choularton, T. W., Dearden, C., and Hill, A.: Modelling the effects of gravity waves on stratocumulus clouds observed during VOCALS-UK, Atmos. Chem. Phys., 13, 7133–7152, https://doi.org/10.5194/acp-13-7133-2013, 2013.

Curry, J. A., Ebert, E. E., and Herman, G. F.: Mean and turbulence structure of the summertime Arctic cloudy boundary layer, Q. J. Roy. Meteor. Soc., 114, 715–746, https://doi.org/10.1002/qj.49711448109, 1988.

de Boer, G., Morrison, H., Shupe, M. D., and Hildner, R.: Evidence of liquid dependent ice nucleation in high-latitude stratiform clouds from surface remote sensors, Geophys. Res. Lett., 38, L01803, https://doi.org/10.1029/2010GL046016, 2011.

de Boer, G., Shupe, M. D., Caldwell, P. M., Bauer, S. E., Persson, O., Boyle, J. S., Kelley, M., Klein, S. A., and Tjernström, M.: Near-surface meteorology during the Arctic Summer Cloud Ocean Study (ASCOS): evaluation of reanalyses and global climate models, Atmos. Chem. Phys., 14, 427–445, https://doi.org/10.5194/acp-14-427-2014, 2014.

de Boer, G., Shupe, M. D., Caldwell, P. M., Bauer, S. E., Persson, O., Boyle, J. S., Kelley, M., Klein, S. A., and Tjernström, M.: Near-surface meteorology during the Arctic Summer Cloud Ocean Study (ASCOS): evaluation of reanalyses and global climate models, Atmos. Chem. Phys., 14, 427–445, https://doi.org/10.5194/acp-14-427-2014, 2014.

Dee, D. P., Uppala, S. M., Simmons, A. J., Berrisford, P., Poli, P., Kobayashi, S., Andrae, U., Balmaseda, M. A., Balsamo, G., Bauer, P., Bechtold, P., Beljaars, A. C. M., van de Berg, L., Bidlot, J., Bormann, N., Delsol, C., Dragani, R., Fuentes, M., Geer, A. J., Haimberger, L., Healy, S. B., Hersbach, H., Hólm, E. V., Isaksen, L., Kållberg, P., Köhler, M., Matricardi, M., McNally, A. P., Monge-Sanz, B. M., Morcrette, J.-J., Park, B.-K., Peubey, C., de Rosnay, P., Tavolato, C., Thépaut, J.-N., and Vitart, F.: The ERA-Interim reanalysis: configuration and performance of the data assimilation system, Q. J. Roy. Meteor. Soc., 137, 553–597, https://doi.org/10.1002/qj.828, 2011.

DeMott, P. J., Prenni, A. J., Liu, X., Kreidenweis, S. M., Petters, M. D., Twohy, C. H., Richardson, M. S., Eidhammer, T., and Rogers, D. C.: Predicting global atmospheric ice nuclei distributions and their impacts on climate, P. Natl. Acad. Sci. USA, 74, 2293–2314, https://doi.org/10.1073/pnas.0910818107, 2010.

Feingold, G., Koren, I., Wang, H., Xue, H., and Brewer, W. A.: Precipitation-generated oscillations in open cellular cloud fields,

Nature, 466, 849–852, https://doi.org/10.1038/nature09314, 2010.

Feingold, G., Koren, I., Yamaguchi, T., and Kazil, J.: On the reversibility of transitions between closed and open cellular convection, Atmos. Chem. Phys., 15, 7351–7367, https://doi.org/10.5194/acp-15-7351-2015, 2015.

Field, P. R., Cotton, R. J., McBeath, K., Lock, A. P., Webster, S., and Allan, R. P.: Improving a convection-permitting model simulation of a cold air outbreak, Q. J. Roy. Meteor. Soc., 140, 124–138, https://doi.org/10.1002/qj.2116, 2014.

Fletcher, J., Mason, S., and Jakob, C.: The Climatology, Meteorology, and Boundary Layer Structure of Marine Cold Air Outbreaks in Both Hemispheres, J. Climate, 29, 1999–2014, https://doi.org/10.1175/JCLI-D-15-0268.1, 2016.

Gray, M. E. B., Petch, J. C., Derbyshire, S. H., Brown, A. R., Lock, A. P., Swann, H. A., and Brown, P. R. A.: Version 2.3 of the Met Office Large Eddy Model: Part II. Scientific Documentation., Tech. rep., 2001.

Harrington, J. Y. and Olsson, P. Q.: On the potential influence of ice nuclei on surface-forced marine stratocumulus cloud dynamics, J. Geophys. Res.-Atmos., 106, 27473–27484, https://doi.org/10.1029/2000JD000236, 2001.

Harrington, J. Y., Reisin, T., Cotton, W. R., and Kreidenweis, S. M.: Cloud resolving simulations of Arctic stratus. Part II: Transition-season clouds, Atmos. Res., 51, 45–75, https://doi.org/10.1016/S0169-8095(98)00098-2, 1999.

Hill, A. A., Field, P. R., Furtado, K., Korolev, A., and Shipway, B. J.: Mixed-phase clouds in a turbulent environment. Part 1: Large-eddy simulation experiments, Q. J. Roy. Meteor. Soc., 140, 855–869, https://doi.org/10.1002/qj.2177, 2014.

Karlsson, J. and Svensson, G.: The simulation of Arctic clouds and their influence on the winter surface temperature in present-day climate in the CMIP3 multi-model dataset, Clim. Dynam., 36, 623–635, https://doi.org/10.1007/s00382-010-0758-6, 2011.

Kay, J. E. and Gettelman, A.: Cloud influence on and response to seasonal Arctic sea ice loss, J. Geophys. Res.-Atmos., 114, D18204, https://doi.org/10.1029/2009JD011773, 2009.

Leonard, B. P., MacVean, M. K., and Lock, A. P.: Positivity-preserving numerical schemes for multidimensional advection, NASA Technical Memorandum, 1993.

Morrison, H., Curry, J. A., and Khvorostyanov, V. I.: A New Double-Moment Microphysics Parameterization for Application in Cloud and Climate Models. Part I: Description, J. Atmos. Sci., 62, 1665–1677, https://doi.org/10.1175/JAS3446.1, 2005.

Morrison, H., de Boer, G., Feingold, G., Harrington, J., Shupe, M. D., and Sulia, K.: Resilience of persistent Arctic mixed-phase clouds, Nat. Geosci., 5, 11–17, https://doi.org/10.1038/ngeo1332, 2012.

Müller, G. and Chlond, A.: Three-dimensional numerical study of cell broadening during cold-air outbreaks, Bound.-Lay. Meteorol., 81, 289–323, https://doi.org/10.1007/BF02430333, 1996.

Myers, T. A. and Norris, J. R.: Observational Evidence That Enhanced Subsidence Reduces Subtropical Marine Boundary Layer Cloudiness, J. Climate, 26, 7507–7524, https://doi.org/10.1175/JCLI-D-12-00736.1, 2013.

Ovchinnikov, M., Korolev, A., and Fan, J.: Effects of ice number concentration on dynamics of a shallow mixed-phase stratiform cloud, J. Geophys. Res.-Atmos., 116, D00T06, https://doi.org/10.1029/2011JD015888, 2011.

Ovchinnikov, M., Ackerman, A. S., Avramov, A., Cheng, A., Fan, J., Fridlind, A. M., Ghan, S., Harrington, J., Hoose, C., Korolev, A., McFarquhar, G. M., Morrison, H., Paukert, M., Savre, J., Shipway, B. J., Shupe, M. D., Solomon, A., and Sulia, K.: Intercomparison of large-eddy simulations of Arctic mixed-phase clouds: Importance of ice size distribution assumptions, J. Adv. Model. Earth Sy., 6, 223–248, https://doi.org/10.1002/2013MS000282, 2014.

Piacsek, S. and Williams, G.: Conservation Properties of Convection Difference Schemes, J. Comp. Physiol., 6, 393–405, 1970.

Prenni, A. J., Harrington, J. Y., Tjernström, M., DeMott, P. J., Avramov, A., Long, C. N., Kreidenweis, S. M., Olsson, P. Q., and Verlinde, J.: Can Ice-Nucleating Aerosols Affect Arctic Seasonal Climate?, B. Am. Meteorol. Soc., 88, 541–550, https://doi.org/10.1175/BAMS-88-4-541, 2007.

Rosenfeld, D., Wang, H., and Rasch, P. J.: The roles of cloud drop effective radius and LWP in determining rain properties in marine stratocumulus, Geophys. Res. Lett., 39, L13801, https://doi.org/10.1029/2012GL052028, 2012.

Sandu, I. and Stevens, B.: On the Factors Modulating the Stratocumulus to Cumulus Transitions, J. Atmos. Sci., 68, 1865–1881, https://doi.org/10.1175/2011JAS3614.1, 2011.

Schröter, M., Raasch, S., and Jansen, H.: Cell Broadening Revisited: Results from High-Resolution Large-Eddy Simulations of Cold Air Outbreaks, J. Atmos. Sci., 62, 2023–2032, https://doi.org/10.1175/JAS3451.1, 2005.

Shipway, B. J. and Hill, A. A.: Diagnosis of systematic differences between multiple parametrizations of warm rain microphysics using a kinematic framework, Q. J. Roy. Meteor. Soc., 138, 2196–2211, https://doi.org/10.1002/qj.1913, 2012.

Solomon, A., Shupe, M. D., Persson, P. O. G., and Morrison, H.: Moisture and dynamical interactions maintaining decoupled Arctic mixed-phase stratocumulus in the presence of a humidity inversion, Atmos. Chem. Phys., 11, 10127–10148, https://doi.org/10.5194/acp-11-10127-2011, 2011.

Solomon, A., Feingold, G., and Shupe, M. D.: The role of ice nuclei recycling in the maintenance of cloud ice in Arctic mixed-phase stratocumulus, Atmos. Chem. Phys., 15, 10631–10643, https://doi.org/10.5194/acp-15-10631-2015, 2015.

Stramler, K., Genio, A. D. D., and Rossow, W. B.: Synoptically Driven Arctic Winter States, J. Climate, 24, 1747–1762, https://doi.org/10.1175/2010JCLI3817.1, 2011.

Trenberth, K. E. and Fasullo, J. T.: Simulation of Present-Day and Twenty-First-Century Energy Budgets of the Southern Oceans, J. Climate, 23, 440–454, https://doi.org/10.1175/2009JCLI3152.1, 2010.

Tripoli, G. J. and Cotton, W. R.: The Use of Ice-Liquid Water Potential Temperature as a Thermodynamic Variable In Deep Atmospheric Models, Mon. Weather Rev., 109, 1094–1102, https://doi.org/10.1175/1520-0493(1981)109<1094:TUOLLW>2.0.CO;2, 1981.

van der Dussen, J. J., de Roode, S. R., and Siebesma, A. P.: How large-scale subsidence affects stratocumulus transitions, Atmos. Chem. Phys., 16, 691–701, https://doi.org/10.5194/acp-16-691-2016, 2016.

Walsh, J. E., Phillips, A. S., Portis, D. H., and Chapman, W. L.: Extreme Cold Outbreaks in the United States and Europe, 1948-99., J. Climate, 14, 2642–2658, https://doi.org/10.1175/1520-0442(2001)014<2642:ECOITU>2.0.CO;2, 2001.

Wang, H. and Feingold, G.: Modeling Mesoscale Cellular Structures and Drizzle in Marine Stratocumulus. Part I: Impact of Drizzle on the Formation and Evolution of Open Cells, J. Atmos. Sci., 66, 3237–3256, https://doi.org/10.1175/2009JAS3022.1, 2009a.

Wang, H. and Feingold, G.: Modeling Mesoscale Cellular Structures and Drizzle in Marine Stratocumulus. Part II: The Microphysics and Dynamics of the Boundary Region between Open and Closed Cells, J. Atmos. Sci., 66, 3257–3275, https://doi.org/10.1175/2009JAS3120.1, 2009b.

Wang, H., Feingold, G., Wood, R., and Kazil, J.: Modelling microphysical and meteorological controls on precipitation and cloud cellular structures in Southeast Pacific stratocumulus, Atmos. Chem. Phys., 10, 6347–6362, https://doi.org/10.5194/acp-10-6347-2010, 2010.

Wood, R., Bretherton, C. S., Leon, D., Clarke, A. D., Zuidema, P., Allen, G., and Coe, H.: An aircraft case study of the spatial transition from closed to open mesoscale cellular convection over the Southeast Pacific, Atmos. Chem. Phys., 11, 2341–2370, https://doi.org/10.5194/acp-11-2341-2011, 2011.

Yamaguchi, T. and Feingold, G.: On the relationship between open cellular convective cloud patterns and the spatial distribution of precipitation, Atmos. Chem. Phys., 15, 1237–1251, https://doi.org/10.5194/acp-15-1237-2015, 2015.

Young, G., Jones, H. M., Choularton, T. W., Crosier, J., Bower, K. N., Gallagher, M. W., Davies, R. S., Renfrew, I. A., Elvidge, A. D., Darbyshire, E., Marenco, F., Brown, P. R. A., Ricketts, H. M. A., Connolly, P. J., Lloyd, G., Williams, P. I., Allan, J. D., Taylor, J. W., Liu, D., and Flynn, M. J.: Observed microphysical changes in Arctic mixed-phase clouds when transitioning from sea ice to open ocean, Atmos. Chem. Phys., 16, 13945–13967, https://doi.org/10.5194/acp-16-13945-2016, 2016.

Young, G., Connolly, P. J., Jones, H. M., and Choularton, T. W.: Microphysical sensitivity of coupled springtime Arctic stratocumulus to modelled primary ice over the ice pack, marginal ice, and ocean, Atmos. Chem. Phys., 17, 4209–4227, https://doi.org/10.5194/acp-17-4209-2017, 2017.